Final Report

Miniature Heat Transport System for Spacecraft Thermal Control

Submitted to:

NASA Goddard Space Flight Center
NASA Contract NAG5-10367

Technical Program Monitor:

Dr. Jentung Ku
NASA Goddard Space Flight Center
Code 545
Greenbelt, MD 20771

(301) 286-3130
Jentung.Ku-1@nasa.gov

by

Dr. Jay M. Ochterbeck
Mechanical Engineering Department
Clemson University
Clemson, SC 29634-0921

(864) 656-3292; (864) 656-4435 Fax
jochter@ces.clemson.edu

Nomenclature

$A_{1,2,3}$	Constants
$Ar = \frac{gL^3\rho(\rho_l - \rho_v)}{\mu^2}$	Archimedes Number
$Bo = \frac{(\rho_l - \rho_v)gd^2}{\sigma}$	Bond Number
$Bi = \frac{h_{conv}}{\lambda / l}$	Biot Number
C	constant
Ca	capillary number
c_p	specific heat
$c_{1,2}$	constants
C_s	Stefan-Boltzmann Constant
$Cu = \frac{\rho v^2}{E_b}$	Cauchy Number
DN	dimensionless number
D	tube inner diameter
D_h	hydraulic diameter
d_1	outer wick diameter
d_2	inner wick diameter
d	diameter
d_w	molecular diameter; Van der Waals Diameter of Liquid Molecule
d_m	mean distance between molecules in liquid
E_b	bulk modulus of fluid
E_i	ionization potential
Fm	figure of merit
$Fr = \frac{\rho v^2}{Lg(\rho_l - \rho_v)}$	Froude Number
$Fr_m = \frac{v^2}{g\beta_t \Delta TL}$	Modified Froude Number
f	function
f_{turb}	friction factor for turbulent flow

G	mass flux
g	acceleration of gravity
$Ga = \frac{gD^3\rho^2}{\mu^2}$	Galileo Number
Go	Goncharov-Kolesnikov Criterion
$Gr = \frac{gL^3\rho^2\beta_t\Delta T}{\mu^2}$	Grashof Number
ΔH	height difference
ΔH_f	enthalpy of fusion
h_{fg}	latent heat of evaporation
h_z	local heat transfer coefficient
h_{tot}	overall heat transfer coefficient
j	superficial velocity
J_{nc}	nucleation rate
$Ja = \frac{h_{fg}}{c_p\Delta T}$	Jacobs Number
k	Boltzmann constant
k_{non-c}	shape correction factor
K	permeability of the wick
K_{td}	dimensionless parameter
$Ko = \frac{h_{fg}\dot{m}}{q_{leak}}$	Kossovich Number
$Kn = \frac{\lambda_{free}}{L}$	Knudsen Number
L	characteristic length
L_{ev}	length of evaporator active zone
l	length
l_w	length of evaporator active zone
l_{lhp}	length of LHP
m	molar mass
$\dot{m}$	mass flow
M	charging mass of working fluid
$Ma = v/v_{sound}$	Mach Number

n_c	critical number of molecules in cluster
N	number density
Na	Avagadro Number
$Nu = \frac{h}{\lambda / l}$	Nusselt Number
$Oh = We^{1/2}/Re$	Ohnesorge Number
P	pressure
$P_{re}=P/P_{cr}$	reduced pressure
$Pr = \frac{c_p \mu}{k}$	Prandtl Number
$Ph = \frac{c_p \Delta T}{h_{fg}}$	Phase Change Number
$Pe = \frac{v \rho c_p}{\lambda / l}$	Peclet Number
Q_{ev}	heat input
q	heat rate
r	radius
r_n	nucleation radios of vapor bubbles
$Ra = \frac{g L^3 \rho^2 \beta_t \Delta T c_p}{\lambda \mu}$	Rayleigh Number
$Re = \frac{\rho j D}{\mu}$	Superficial Reynolds Number
$Re = \frac{\rho v d}{\mu}$	Reynolds Number
S	area
$Su = \frac{\rho L \sigma}{\mu^2}$	Suratman Number
T	temperature
t	time
V	volume
V_{loop}	LHP total volume
V_m	effective molecular volume of liquid
v	velocity
$We = \frac{\rho L v^2}{\sigma}$	Weber Number

X	Lochart-Martinelli Parameter
x	vapor quality
z	coordination number
α	void fraction, polarizability
Δ	difference between values
ε	porosity
ε_o	potential parameter
ε_m	potential energy
ε_w	pseudo- convection coefficient
ε_o	potential parameter
ρ	fluid density
ρ_{Lc}	liquid density (cold case)
ρ_{Vc}	vapor density (cold case)
ρ_{Lh}	liquid density (hot case)
ρ_{Vh}	vapor density (hot case)
β	fraction of CC volume occupied by liquid (cold case), accommodation coefficient
β_t	thermal expansion coefficient
α	void fraction of CC volume (hot case)
μ	dynamic viscosity
λ	thermal conductivity
λ_{free}	mean free path
δ	thickness
Π	disjoining pressure, dimensionless group
σ	surface tension
θ	contact angle

Subscripts

b	boiling
c	condenser
cap	capillary

char	characteristic
cr	critical
eff	effective
eq	equivalent
ev	evaporator
hp	heat pipe
i	wick inner, interface
LHP	Loop Heat Pipe
l	liquid
M	model
max	maximum
mbl	microgravity Bond length
o	output, wick outer
P	prototype
p	wick pore
s	superficial, solid
sh	superheat
td	Taitel-Dukler
tot	total
tt	turbulent-turbulent
v	vapor
vg	vapor collecting grooves
w	wall

Introduction

Loop heat pipes (LHP) are efficient devices for heat transfer and use the basic principle of a closed evaporation-condensation cycle. The advantage of using a loop heat pipe over other conventional methods is that large quantities of heat can be transported through a small cross-sectional area over a considerable distance with no additional power input to the system. By using LHPs, it seems possible to meet the growing demand for high-power cooling devices. Although they are somewhat similar to conventional heat pipes, LHPs have a whole set of unique properties, such as low pressure drops and flexible lines between condenser and evaporator, that make them rather promising.

LHPs are capable of providing a means of transporting heat over long distances with no input power other than the heat being transported because of the specially designed evaporator and the separation of liquid and vapor lines. The correlation of the geometrical, structural, and physicochemical properties of the LHP elements and of the working fluid plays a key role in helping LHPs successfully and reliably start-up and operate in a required range of temperatures, given specific heat loads, and ambient conditions. For LHP design and fabrication, preliminary analysis on the basis of dimensionless criteria is necessary because of certain complicated phenomena that take place in the heat pipe.

Modeling the performance of the LHP and miniaturizing its size are tasks and objectives of current research. In the course of this work, the LHP and its components, including the evaporator (the most critical and complex part of the LHP), were modeled with the corresponding dimensionless groups also being investigated. Next, analysis of heat and mass transfer processes in the LHP, selection of the most weighted criteria from known dimensionless groups (thermal-fluid sciences), heat transfer rate limits, (heat pipe theory), and experimental ratios which are unique to a given heat pipe class are discussed.

In the third part of the report, two-phase flow heat and mass transfer performances inside the LHP condenser are analyzed and calculated for Earth-normal gravity and microgravity conditions. On the basis of recent models and experimental databanks, an analysis for condensing two-phase flow regimes, pressure gradients, and local heat transfer coefficients using ammonia, propylene, and R134, are carried out.

LHP Component Scaling

The fluid flow and heat transfer in the scaled model and in the original will be equivalent only if the velocity, temperature, and pressure fields are identical, making the scaling a very complicated issue. To enforce the identity of velocity, temperature, and pressure fields, the dimensionless numbers describing the problem must be equal for the model and for the original. Eighteen dimensionless groups are considered crucial for the thermal-gravitational scaling of two-phase loops [1]. An 18-number approach is not a limit. The actual number depends on the depth of the physical problem consideration and on the number of selected physical parameters. There is perfect similarity between the model and the original if all dimensionless numbers are identical for both. Obviously, this cannot be achieved for two-phase flow and heat transfer, because the governing phenomena are too complex and the number of dimensionless numbers too large.

Table 1-Governing Parameters for LHP Elements

LHP Element	Important Phenomena	Governing Parameters
Liquid line	Heat exchange Pressure loss	$\dot{m}, c_{p,l}, \lambda_l, \mu_l$ $\nu_l, \dot{m}, \rho_l, d_l, l_l, g, \Delta H$
Compensation Chamber	Heat exchange	$\dot{m}, p_v(T), c_{p,l},$ $c_{p,v}, \lambda_l, \lambda_w$
Evaporator	Evaporation Pressure loss (wick structure) Capillary head Pressure loss (vapor grooves) Heat exchange	$\dot{m}, h_{fg}, T_v \rightarrow \delta_w, r_{ev}, l_{ev}$ $\dot{m}, K, r_{eff}, \delta_w, \nu_l$ σ, r_{eff}, θ $\dot{m}, S_{vg}, l_{vg}, n_{vg}, \nu_v$ $\dot{m}, c_{pl}, c_{pv}, \lambda_l, \lambda_v, \lambda_w$
Vapor Line	Heat exchange Pressure loss	$\dot{m}, c_{p,v}, \lambda_v, \mu_v$ $\nu_v, \dot{m}, \rho_v, d_v, l_v$
Condenser & Subcooler	Heat exchange Pressure loss	$\dot{m}, h_{fg}, c_{pl}, r_c, l_c, r_s, l_s$ $\nu_l, \dot{m}, \rho_l, r_c, l_c, r_s, l_s$

Distorted scaling offers some possibilities, when not the entire LHP but only elements of the LHP are involved. Distorted (or imperfect) scaling also can lead to useful results because there are parameters that have only a minor influence: for instance, the Mach number for incompressible flow or the Froude

number for pure vapor flow. In addition, the geometric distortion is impractical when the length scaling leads to excessively small (capillary) conduits in the model. However, for studies of boundary layer effects and boiling heat transfer, a geometric distortion is not permitted, since the surface roughness is very important in such problems. The governing parameters for the main phenomena in the LHP section are presented in Table 1.

Liquid and Vapor Line Scaling

If the Buckingham π-Theorem for liquid line scaling is applied, the dimensionless formulations of pressure loss and temperature change phenomena can be stated as:

$$\frac{\Delta p}{\rho v^2} = f\left(Re_l, \frac{l_l}{d_l}, Fr_l, \cos(\psi)\right) \tag{1}$$

$$\frac{\Delta T_{io}}{\Delta T_{ca}} = f\left(\frac{h_{tot}\Delta T_{ca}}{\rho_l l_l v^3}, \frac{c_{pl}\Delta T_{ca}}{v^2}\right) \tag{2}$$

where ΔT_{io} is the working fluid temperature drop between the points where the fluid enters and leaves the liquid line; ΔT_{ca} is the temperature difference between the fluid at the end of condenser and the ambient; h_{tot} is the overall heat transfer coefficient between the ambient and the working fluid in the liquid line.

One of the purposes of this scaling work was a reduction of the size of all the components of the LHP. Therefore, a reduction of radius and length of the liquid line in particular were necessary. Reducing the radius has only a very small effect on the temperature change. When reducing the radius, while keeping the mass flow rate through the liquid line constant, the velocity of the liquid has to increase. Hence, the temperature change decreases, which in turn usually has a positive effect on the performance of the LHP. Due to this behavior, a first look at the pressure drop across the liquid line is made. For perfect similitude, all non-dimensional numbers must be identical for the original and the model. Assuming no change in gravity or the orientation in the gravity field, the Reynolds number, the Froude number, and the length to diameter ratio must be the same for both versions of the liquid line. Mathematically, this can be expressed for two working fluids (x and y) as follows:

$$\begin{gathered}\left[Re_l\right]_x = \left[Re_l\right]_y \qquad \left[Fr_l\right]_x = \left[Fr_l\right]_y \\ \left[l_l/d_l\right]_x = \left[l_l/d_l\right]_y\end{gathered} \tag{3}$$

In these equations, the velocity of the fluid can be expressed as:

$$v = \frac{4\dot{m}}{d^2\pi\rho} = \frac{4Q_{ev}}{d^2\pi\rho h_{fg}} \tag{4}$$

This leaves three parameters to satisfy the conditions for similitude with respect to pressure drop: liquid line diameter, length, and heat input to the evaporator Q_{ev}. After mathematical reorganization of Eq. (3) the following are expressions for d_l, l_l, and Q_{ev}:

$$\frac{d_x}{d_y} = \left(\frac{\mu_x}{\mu_y}\right)^{2/3}\left(\frac{\rho_y}{\rho_x}\right)^{2/3} \qquad \frac{l_x}{l_y} = \frac{d_x}{d_y} \qquad \frac{Q_{ev,x}}{Q_{ev,y}} = \frac{d_x}{d_y}\frac{\mu_x}{\mu_y}\frac{h_{fg,x}}{h_{fg,y}} \tag{5}$$

Figure 1 shows the ratio for the diameter and also for the length for three different working fluids with respect to ammonia. The shape of the curves in Fig. 1 is mainly due to the ratio μ_x/μ_y, which shows the same behavior as a function of temperature. The ratio of the densities has only a minor influence on the shape of the curves because its variation with temperature is relatively small.

Table 2 shows the results of scaling using the five working fluids presented. The results were calculated for an ammonia LHP with a liquid line length of l_l = 0.7 m, a liquid line diameter of d_l = 3 mm, and an evaporator heat input of Q_{ev} = 30 W.

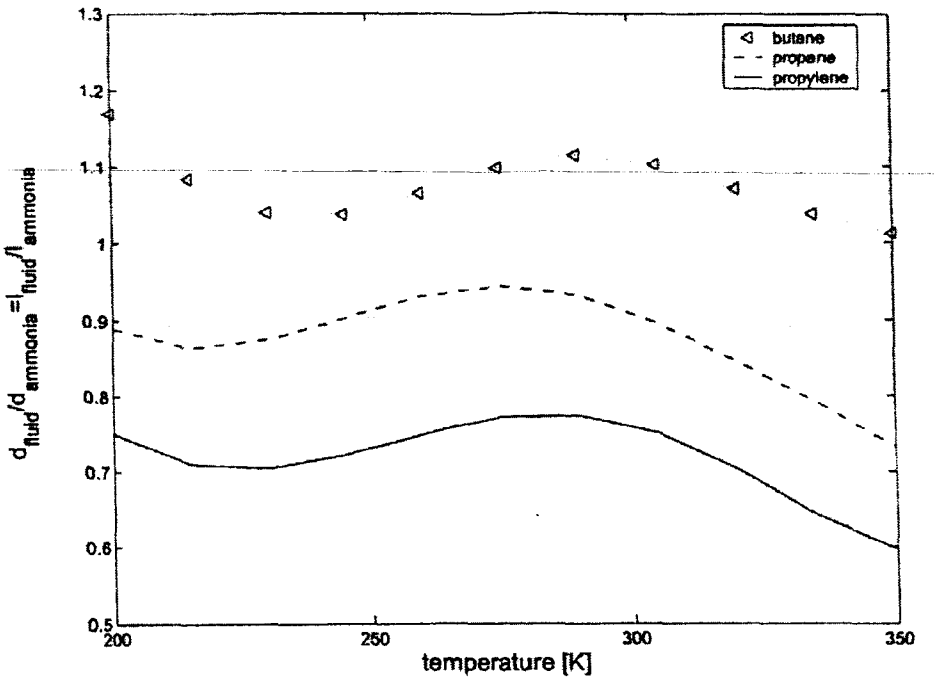

Fig. 1. Ratios of line diameters for three working fluids as a function of temperature

Depending on the working fluids used, there is a broad range of scaling possibilities. For the presented fluids, the line diameter could be scaled in the range from 0.775 to 2.68 times the diameter of a liquid line designed for ammonia. At the same time, the heat input to the evaporator has to be adjusted. This can be done in a range from 0.0001 to 39.38 times the value for ammonia LHP. The temperature change has been also documented in Table 2. It shows that the change in temperature is only minor. When scaling the liquid line, the focus was on the pressure drop because this limits the transport capacity of the LHP. The change in temperature was considered to be a minor effect, which also is justified by the results. The temperature change was calculated for two different cases. While the line diameter, the length of the line, and the heat input to the evaporator of the ammonia version were kept constant, the ambient temperature was varied to show the influence on temperature change. The change, ΔT_1, was calculated for an ambient temperature of 303.15K. The change, ΔT_2, was calculated for an ambient temperature of 333.15K. The condenser exit temperature was kept at a constant 274.15K for all calculations. The results show that the temperature change of the scaled liquid line is always smaller than the temperature change in the ammonia case.

Table 2-Liquid line scaling results at $T = 290$ K

Fluid	Scaling factor d_i	Scaling factor Q_{sw}	$\frac{\Delta p}{\rho v^2}$	ΔT_1 K	$h_{tot,1}$ W/mK	ΔT_2 K
Water	2.62	39.4	2.035×10^5	0.68	0.025	1.4
Butane	1.11	0.390	2.035×10^5	1.45	0.005	2.39
Propane	0.932	0.305	2.035×10^5	1.75	0.005	3.53
Propylene	0.775	0.133	2.035×10^5	2.86	0.005	5.78
Ammonia	1	1	2.035×10^5	3.05	0.018	6.34
Methanol	1.45	2.89	2.035×10^5	0.66	0.009	1.35

By analogy to liquid line scaling, the vapor line scale analysis can be made. The influence of gravity for this case can be neglected. Doing so will simplify the expression for pressure drop and reduce the number of independent dimensionless numbers to two (Re_v and l_v/d_v). Thus, only one parameter has to be adjusted to yield similitude with respect to the pressure drop.

LHP Evaporator Scaling

Deriving non-dimensional numbers for the evaporator

Scaling of the LHP evaporator and its elements is a far more complicated problem. The results will have a strong dependence on simplifications and suggestions that would be made during governing parameter selection and analysis of the heat and mass transfer processes in this LHP element. Attempting to take into account every parameter (without performing an analysis of its significance) confuses the problem and can lead to the conclusion that simultaneous thermal and hydraulic LHP scaling might even be impossible.Scaling generally can be done with respect to several aspects, e.g. geometrical scaling, fluid to fluid scaling, or gravitational scaling. Based on models, non-dimensional groups that can be used to evaluate scaling issues were derived and the possibility of scaling was evaluated.

The evaporator is the most complex part of the LHP. There are basically two geometric configurations used for the evaporator:

- Plate evaporator
- Cylindrical evaporator

In this work, we focus on the cylindrical configuration, because it is the most common version. A schematic of the cylindrical evaporator is shown in Fig. 2. A number of important, non-dimensional groups for a certain scaling approach also depend on the physical phenomena considered relevant for a certain application.

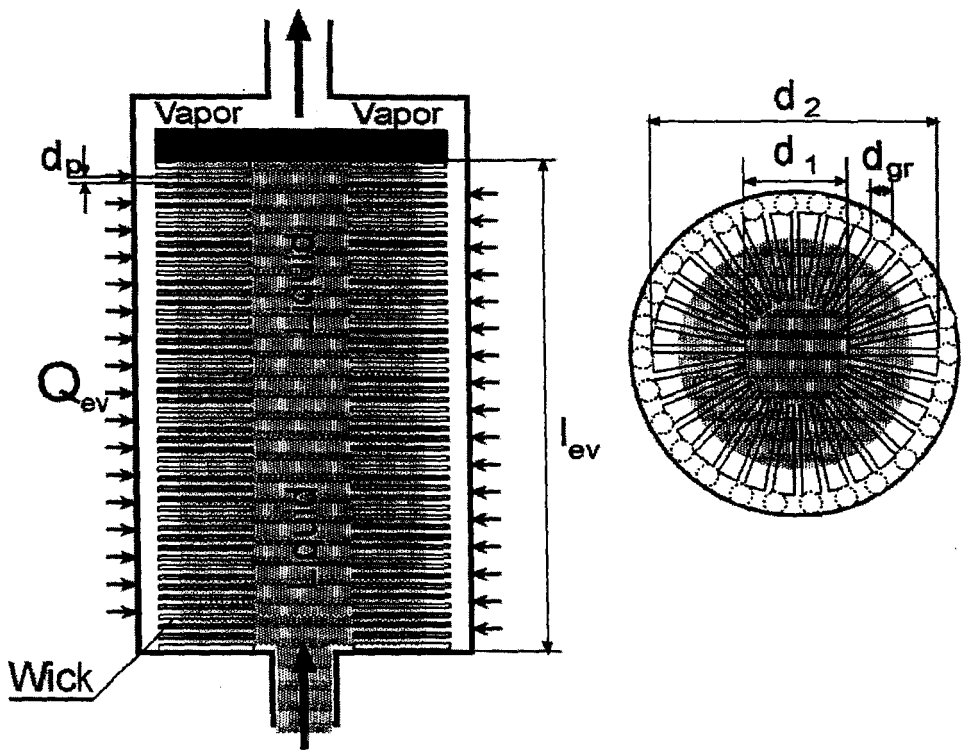

Fig. 2 Model of LHP evaporator

Perfect similitude between model and original can be achieved only if all 18 [1] non-dimensional groups are identical for both. Because not all 18 non-dimensional are equally relevant, ignoring physical phenomena that are of minor importance can lead to useful results. Though such an approach necessarily leads to imperfect or distorted scaling, considering a scaled evaporator, perfect scaling seems to be impossible due to the high number of non-dimensional groups that must be considered and due to technological problems. I.e. A geometric distortion must be accepted because perfect scaling can lead to impractical small-capillary conduits.

We based our scaling approaches on two different models for the evaporator. Because the equations derived for those models were non-dimensionalized, the physical phenomena implemented in the models should also considered important for the scaling process.

The first model is based on a model presented by Kiseev, et al. [2]. It is a one-dimensional model, derived from the one-dimensional energy equation (see Appendix 1), that allows for the calculation of

the temperature in the compensation chamber, the vapor temperature, and the temperature difference between the vapor and the fluid returning to the compensation chamber from the condenser:

$$\frac{d^2\bar{T}}{d\bar{r}^2}+\frac{1}{\bar{r}}(1-\varepsilon_w)\frac{d\bar{T}}{d\bar{r}}=0 \qquad (6)$$

There are several assumptions made in the model:

- The temperature in the compensation chamber equals the temperature on the inside of the wick. This is valid under non-zero g conditions when natural convection leads to the equalization of the temperature in the compensation chamber.
- Filtration of working fluid through the capillary structure to the evaporation surface as well as the heat transfer is realized only in a radial direction. This assumptions holds if the evaporator length is longer than the diameter and the wick is completely flooded.
- The Clausius-Clapeyron equation can be used, which requires that the compensation chamber is partly filled with saturated vapor. This case occurs usually in the autoregulation regime of the LHP.

Non-dimensional groups describing the temperature distribution in the wick were derived by non-dimensionalizing the corresponding equations and using their boundary conditions as suggested by Fershtater and Maidanik [3].

The solution of Eq. (6) describes the non-dimensional temperature distribution in the wick of the evaporator:

$$\bar{T}(\bar{r})=\bar{r}^{\varepsilon_w}, \qquad (7)$$

where

$$\bar{r}=\frac{r}{r_o}, \quad \bar{T}=\frac{T-T_{cc}}{T_v-T_{cc}}, \qquad (8)$$

$$\varepsilon_w=\frac{q_{ev}c_p r_o}{\lambda_{eff}(h_{fg}+c_p(T_v-T_{cc}))}, \quad r_o=\frac{d_2}{2}+d_{gr} \qquad (9)$$

Thus, to have thermal similitude in model and original, it is necessary to have the same non-dimensional coordinate $\bar{r}$ and the same exponent ε_w:

$$\left[\frac{r}{r_o}\right]_M = \left[\frac{r}{r_o}\right]_P \tag{10}$$

$$\left[\varepsilon_w\right]_M = \left[\varepsilon_w\right]_P \tag{11}$$

Equations (10) and (11) lead to a similitude in the temperature field of prototype and model.

Figure 3 shows the effect on the non-dimensional temperature as a function of non-dimensional coordinate with variations of the effective wick conductivity λ_{eff} (assuming the wick is completely saturated with liquid).

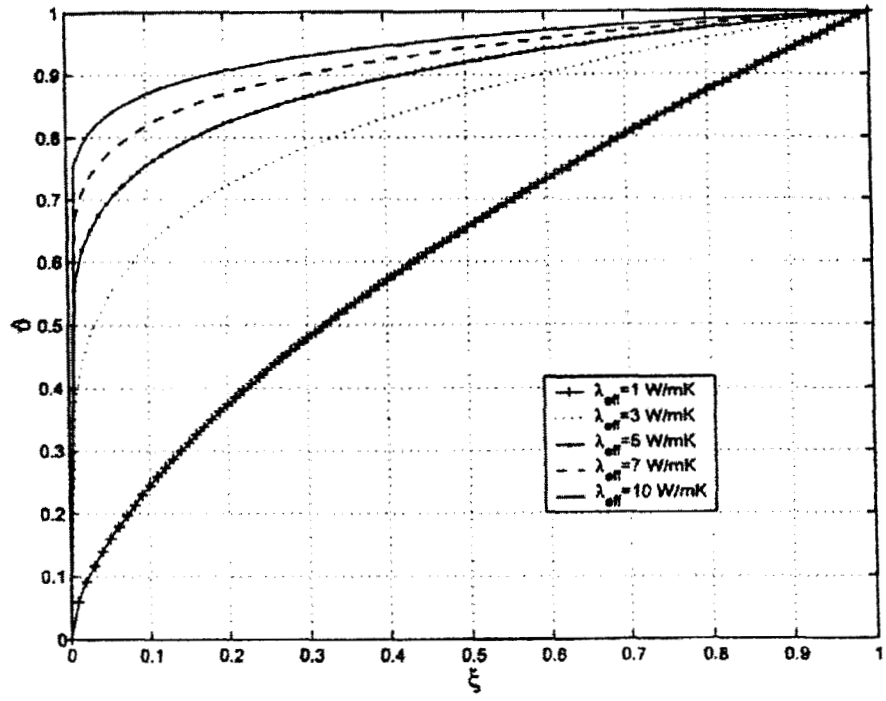

Fig.3. Non-dimensional Temperature Field in the Wick for Different λ_{eff}; Working Fluid – Ammonia.

The full range of $\bar{r}$ plotted in the Fig. 3, in other words, as $\bar{r}$ approaches zero, is not used in actual LHPs, but it gives some insight into the behavior of the temperature when the ratio of the inner and outer radii of the wick approaches extremes. For high effective conductivities of the saturated wick, the non-dimensional temperature $\bar{T}$ shows a steep gradient as $\bar{r}$ approaches zero, while, for low conductivities, this is not the case. This behavior is caused by the influence of ε_w on the solution. High values of λ_{eff} result in lower values of ε_w and thus cause a lower temperature gradient on the outside of the wick.

However, because the temperature at $\bar{r} = 0$ has to be zero according to the model, a steeper temperature gradient is necessary in this case.

Using fluid to fluid scaling, thermal similitude can be achieved when the outer diameter r_o is changed to ensure that Eq. (11) is satisfied. The ratio for the outer diameter of prototype and model is in this case given by:

$$\frac{[r_o]_M}{[r_o]_P} = \frac{[q_{ev}c_p]_P}{[q_{ev}c_p]_M} \frac{[\lambda_{eff}(h_{lg} + c_p(T_v - T_{cc}))]_M}{[\lambda_{eff}(h_{lv} + c_p(T_v - T_{cc}))]_P} \tag{12}$$

The conductivity of the saturated wick λ_{eff} in the general case is a function of the porosity, the conductivity of the wick material, and the conductivity of the fluid. Figure 4 shows the ratio $[r_o]_M / [r_o]_{ammonia}$ for two different working fluids. When changing the outer radius of the wick r_o, the inner radius r_i has to be changed accordingly, otherwise the non-dimensional coordinate will not be the same for prototype and model. With the change of the radii, a change of the total heat input to evaporator Q_{ev} occurs, if the specific heat input is kept constant.

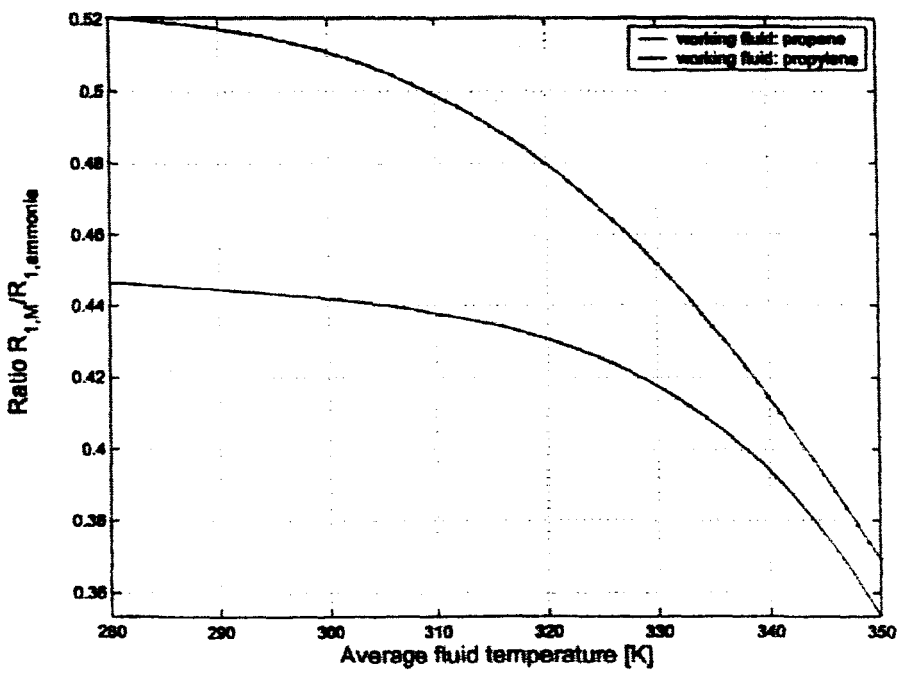

Fig. 4 Scaling factors for the evaporator radius.

When it is necessary to keep Q_{ev} constant, another expression relating the lengths of prototype and model can be found that has to be satisfied for thermal similitude:

$$\frac{[l_{ev}]_M}{[l_{ev}]_P} = \frac{[c_p]_M}{[c_p]_P} \frac{[\lambda_{eff}(h_{fg} + c_p(T_v - T_{cc}))]_P}{[\lambda_{eff}(h_{fg} + c_p(T_v - T_{cc}))]_M} \tag{13}$$

The pressure drop in the evaporator consists of the pressure drop in the wick and in the vapour removal grooves. Taking into account that wick pressure drop can be calculated using the Darcy's law and $\Delta p = f(\rho, r_o, r_i, l_{ev}, \mu, v_o, K)$, non-dimensional groups for the pressure drop in the wick structure can be derived using the Buckingham-Π-theorem:

$$\Pi_{w1} = \frac{\Delta p_w}{\rho v_o^2} \tag{14}$$

$$\Pi_{w2} = \frac{\mu_l}{\rho v_o R_o} \tag{15}$$

$$\Pi_{w3} = \frac{l_{ev}}{R_o} \tag{16}$$

$$\Pi_{w4} = \frac{K}{R_o^2} \tag{17}$$

$$\Pi_{w5} = \frac{R_i}{R_o} \tag{18}$$

where v_o is the radial fluid velocity on the outer radius of the wick, Π_{w1} is the Euler number, Π_{w2} is the inverse Reynolds number, and K is the wick permeability.

The non-dimensional groups for the pressure drop in the vapor grooves also can be obtained by using the Buckingham-Π-theorem:

$$\Pi_{vg1} = \frac{\Delta p_{vg}}{\rho v_e^2} \tag{19}$$

$$\Pi_{vg2} = \frac{\mu_v}{\rho v_e D_h} \tag{20}$$

$$\Pi_{vg3} = \frac{l_{ev}}{D_h} \tag{21}$$

$$\Pi_{vg4} = \frac{S_{vg,tot}}{D_h^2} \tag{22}$$

$$\Pi_{vg5} = k_{non-c} \tag{23}$$

where v_e is the fluid velocity at the end of the vapor grooves, Π_{vg1} is the dependent non-dimensional group, Π_{vg2} is the inverse Reynolds number for the vapor grooves, D_h is the hydraulic diameter of one vapor groove, $S_{vg,tot}$ is the total cross-sectional area of the vapor grooves, and k_{non-c} is a shape factor that accounts for non-circular vapor grooves.

Because Eq. 18 can also be derived from Eq. 7, and Eqs. 14 and 19 are dependent non-dimensional groups, there are nine non-dimensional groups that must be identical for prototype and model.

Geometrical Scaling of the Evaporator

Geometrical scaling can be used to derive a miniature model of an existing LHP that works with the same fluid used inthe original version. Based on the nine non-dimensional groups presented in the previous paragraph, an approach for geometrical scaling is derived as follows. Equation (12) can be used to calculate the ratio between the outer radii r_o of model and prototype. If the same working fluid is used and the effective conductivity of the wick λ_{eff} is kept constant, this equation can be simplified to:

$$\frac{[R_o]_M}{[R_o]_P} = \frac{[q_{ev}]_P}{[q_{ev}]_M} \tag{24}$$

which relates the heat input density and the outer radii.

Using Eq. (18), the inner radius of the wick structure can be determined:

$$R_{i,M} = R_{o,M}\left[\frac{R_i}{R_o}\right]_P \tag{25}$$

Thus, thermal similitude (according to the model) is ensured, leaving hydraulic similitude as a second requirement to be fulfilled. Using the third non-dimensional group for the pressure drop in the wick, the length of the scaled evaporator can be calculated:

$$l_{ev,M} = l_{ev,P} \frac{R_{o,M}}{R_{o,P}} \tag{26}$$

It can be shown that the inverse Reynolds number is the same for model and prototype if Eqs. (24), (25), and (26) are satisfied. Having defined length, outer diameter, and specific heat input for the scaled evaporator, it can be shown that the total heat input for model and evaporator have the following ratio:

$$\frac{Q_{ev,M}}{Q_{ev,P}} = \frac{R_{o,M}}{R_{o,P}} \tag{27}$$

The fourth non-dimensional group derived for the pressure drop in the wick (Eq. [17]) has to be used to determine the permeability of the scaled wick structure K_M:

$$\frac{K_M}{K_P} = \frac{R_{o,M}^2}{R_{o,P}^2} \tag{28}$$

The permeability of the wick structure is most likely to limit the scaling range, since the permeability of the wick has to be changed while the conductivity remains constant.

Peterson [4] states the following relations for conductivity and permeability with respect to pore diameter d_p and porosity ε (wick is assumed to be modelled by packed spheres):

$$K = \frac{\left(\frac{d_p}{2}\right)^2 \varepsilon^2}{37.5(1-\varepsilon)^2} \tag{29}$$

$$\lambda_{eff} = \frac{\lambda_l(2\lambda_l + \lambda_w) - 2(1-\varepsilon)(\lambda_l - \lambda_w)}{(2\lambda_l + \lambda_w) + (1-\varepsilon)(\lambda_l - \lambda_w)} \tag{30}$$

When geometric scaling is considered, the permeability K can be adjusted by changing the pore diameter of the wick while keeping the porosity constant. Thus, the conductivity also remains constant.

By using the non-dimensional groups for the pressure drop in the vapor grooves, the dimensions of the vapor grooves in the scaled evaporator can be determined. From Eq. (11), the hydraulic diameter of the model vapor grooves can be obtained:

$$D_{h,M} = \frac{l_{ev,M}}{l_{ev,P}} D_{h,P} \tag{31}$$

The condition that the Reynolds number in the vapor grooves has to be the same for model and prototype, results in an equation for total cross-sectional area of the vapor grooves:

$$\frac{\left[S_{vg,tot}\right]_M}{\left[S_{vg,tot}\right]_P} = \frac{D_{h,M}^2}{D_{h,P}^2} = \frac{R_{o,M}^2}{R_{o,P}^2} \tag{32}$$

The same condition can also be derived form Eq. (22).

Thus, the last parameter to be calculated is the shape correction factor k_{non-c}. This correction factor accounts for variations in the vapor groove pressure drop as a result of the non-circular shape of the vapor grooves. It only can be the same for model and prototype if the shape of the vapor grooves is the same for both.

So far, we have presented the steps that lead to a similitude of the temperature field and the pressure drop in the wick and the pressure drop in the vapor grooves. In addition, in Table 1, the capillary head is mentioned to be an important phenomenon. When the same working fluid and the same material for the wick structure in model and protoype are used, the surface tension σ and the contact angle θ do not change. If the scaling is used to derive a miniature LHP, Eq. (29) states that the permeability of the wick has to be reduced by decreasing the pore diameter of the wick. This, in turn, leads to a higher capillary head, which consequently has a positive effect on the capillary limit of the LHP. Also, in Table 1, the heat transfer is considered to be an important phenomenon. Because the same working fluid is used for geometric scaling and the effective conductivity of the wick is kept constant, there is only a change in the mass flow rate. The Reynolds-number, however, is kept constant so that the heat transfer coefficient for the forced convection inside the vapor grooves is the same in both model and prototype.

The second model used for evaporator scaling is a two-dimensional model based on the energy balance equation:

$$\frac{d^2\bar{T}}{d\bar{r}^2} + \frac{1}{\bar{r}}(1-\varepsilon_w)\frac{d\bar{T}}{d\bar{r}} + \frac{d^2\bar{T}}{d\bar{z}^2} = 0 \tag{33}$$

where $\bar{z} = \frac{z}{r_o}$. It is not necessary to know the analytical solution of the Eq. (33) in order to find non-dimensional groups that must have the same value for model and prototype. The non-dimensional groups can be derived directly from the Eq. (33). For similitude in the temperature distribution, the necessary non-dimensional groups are:

$$\Pi_{w1} = \frac{T - T_{cc}}{T_v - T_{cc}} \tag{34}$$

$$\Pi_{w2} = \varepsilon_w = \frac{q_{ev} c_p r_o}{\lambda_{eff}(h_{fg} + c_p(T_v - T_{cc}))} \tag{35}$$

$$\Pi_{w3} = \varepsilon_l = \frac{q_{ev} c_p r_o}{\lambda_l(h_{fg} + c_p(T_v - T_{cc}))} \tag{36}$$

$$\Pi_{w4} = \frac{R_i}{R_o} \tag{37}$$

$$\Pi_{w5} = \frac{l_{ev}}{R_o} \tag{38}$$

By comparing the non-dimensional groups derived for the two-dimensional model with the ones derived for the one-dimensional model, it can be seen that there are two more groups for the two-dimensional model: Π_{w5} and Π_{w3}. The first group expresses the aspect-ratio of the evaporator. Obviously, this group is not necessary for a one-dimensional model. The second group expresses the pseudo-convection in the core. For geometric scaling, this group has the same behavior as Π_{w2}.

Therefore, there are two more non-dimensional groups that must be the same for model and prototype to achieve similitude in the temperature distributions using the two-dimensional model. However, as previously derived, Π_{w5} also appears as a non-dimensional group for the pressure drop in the wick. Hence, geometric scaling based on the one-dimensional model and geometric scaling based on the two-dimensional model lead to (practically) the same results.

In addition, a scaling using a more detailed two-dimensional model was made. The model was based on constitutive laws for mass (continuity equation), momentum (Navier-Stokes equation for z- and r-directions) and energy. The scaling equations derived from this model are basically the same as the equations derived from the one-dimensional model.

Appendix 1. Formulation of one-dimensional heat conduction equation for evaporator

General form of local instantaneous internal energy equation is:

$$\frac{\partial}{\partial t}(\rho u) = -\nabla \cdot \rho u \vec{v} - \nabla \cdot \vec{q} - p \nabla \cdot \vec{v} - \vec{\tau} : \nabla \vec{v}$$

Evaporator Model Assumptions:

1. Steady-state regime $\rightarrow \frac{\partial}{\partial t} \equiv 0$;
2. Incompressible fluid $\rightarrow \rho = const$ and from local instantaneous mass balance equation $\nabla \cdot \vec{v} = 0$;
3. Viscous dissipation is negligible $\vec{\tau} : \nabla \vec{v} = 0$;

$$\Rightarrow \qquad \rho \vec{v} \cdot \nabla u + \nabla \cdot \vec{q} = 0;$$

4. Purely radial flow (one-dimensional model) in cylindrical coordinates:

$$\vec{v} = \begin{bmatrix} v_r \\ 0 \\ 0 \end{bmatrix} \qquad \nabla u = \begin{bmatrix} \partial u / \partial r \\ 0 \\ 0 \end{bmatrix} \qquad \nabla \cdot \vec{q} = \frac{1}{r}\frac{\partial}{\partial r}(r q_r)$$

$$\Rightarrow \qquad \rho v_r \frac{du}{dr} + \frac{1}{r}\frac{d}{dr}(r q_r) = 0$$

5. $c_p = const$;
6. Fourier fluid $\rightarrow q_r = -\lambda \frac{dT}{dr}$;

$$\Rightarrow \qquad \rho c_p v_r \frac{dT}{dr} - \frac{1}{r}\frac{d}{dr}\left(r\lambda \frac{dT}{dr}\right) = 0$$

But:

$$\rho v_r \equiv \frac{\dot{m}}{2\pi r L_{ev}} = \frac{1}{2\pi r L_{ev}} \frac{Q_{ev}}{h_{fg} + c_p (T_v - T_{cc})} = \frac{1}{2\pi r L_{ev}} \frac{q_{ev} 2\pi r_o L_{ev}}{h_{fg} + c_p (T_v - T_{cc})} = \frac{q_{ev} r_o}{r\left[h_{fg} + c_p (T_v - T_{cc})\right]}$$

7. $\lambda = const$

Then, the final equation is:

$$\frac{d^2 T}{dr^2} + \frac{1}{r}(1 - \varepsilon_w)\frac{dT}{dr} = 0$$

where the pseudo-convection coefficient is given by:

$$\varepsilon_w = \frac{q_{ev} r_o c_p}{\lambda\left[h_{fg} + c_p (T_v - T_{cc})\right]} = \frac{q_{ev} r_o}{\lambda\left[\frac{h_{fg}}{c_p} + (T_v - T_{cc})\right]}$$

LHP DIMENSIONLESS CRITERIA

Dimensionless analysis is very important for practical applications in engineering because of its ability to reduce the complexity of physical problems to a simple ocular form. This approach is very appealing because it allows engineers and scientists to understand more deeply the physical point of investigated phenomena and to obtain first results and estimations quickly, prior to quantitative modeling. Dimensionless numbers and criteria occupy a very honored place in heat- and mass- transfer theory and particularly in the theory behind heat pipes. Dimensionless analysis allows for the estimation of heat pipe mass and geometrical and operational characteristics, for the selection of primary heat and mass transfer processes in specific heat pipes, and for the discovery of the temperature and heat load functional diapasons for the heat pipe.

The specially designed evaporator and separated liquid and vapor lines are distinguishing features of the Loop Heat Pipes (LHP) as a unique class of heat transfer devices. Dimensionless analysis is extremely necessary for the LHP because of the complicated phenomena that take place there, including: (1) counter heat- and fluid- flows in the capillary wick of the evaporator, (2) liquid and vapor filtration through microporous structures, (3) intensive phase change processes inside the wick, in vapor collecting channels of the evaporator, and in the condenser, (4) heat transfer by convection, conduction, and radiation, (5) evaporation from the inverted meniscus, (6) the moving, non-equilibrium vapor-liquid interface, (7) the strong influence of gravitational, inertial, viscous, and capillary forces. The correlations of geometrical, structural, and physicochemical properties of the LHP evaporator elements (primary and secondary wicks, compensation chamber, vapor collecting grooves), the condenser, liquid/vapor lines, and the working fluid play key roles for LHP reliable start-up and successful operation in the required range of temperatures, heat loads, and ambient conditions.

According to the theory of dimensional analysis, the following are ways to identify dimensionless groups that are important for a given physical process or phenomenon. First, a formal and well-known method involves the appearance of the dimensionless groups after the non-dimensionalizing of conservation equations. The formalism of this approach is its major disadvantage. Researchers often have difficulties with the physical interpretation of some dimensionless groups when using this method. In addition, results depend strongly on the initial set of parameters chosen as basic for the non-dimensionalizing operation. The use of the Buckingham π-Theorem is the second, informal technique. This method is powerful (and very elegant) but requires detailed knowledge of the investigated subject and physical insight [5]. The first and most responsible step of the method involves choosing important physical parameters (see Table 1.). One problem with the technique is that the choices made in order to derive dimensionless groups are not unique. It takes either intuition or trial and error to find parameters that have physical meaning. That the application of the Buckingham π-Theorem and the non-

dimensionalizing of conservation equations for LHP distorts scaling when only elements of the heat pipe (not the entire LHP) are involved was demonstrated in the previous chapter.

In the present section, the semi-empirical approach was used for the determination of critical dimensionless groups for the LHP evaporator. The essence of the approach is the analysis of heat and mass transfer processes in the evaporator and the selection of the most significant criteria from known dimensionless groups (thermal-fluid sciences), heat transfer rate limits (heat pipe theory), and experimental ratios that are unique for given classes of heat pipes. This approach is rather informal and itself includes the Buckingham π-Theorem method in its general case as a powerful tool for the selection of important similarity numbers derived from the same starting point.

Table 3 - Dimensionless criteria for loop heat pipes (LHPs)

Name	Description	Function
	Functional	
Fluid selection	Ratio between Vapor-Liquid Figures of Merit for two working fluids: $\frac{[Fm_{vl}]_x}{[Fm_{vl}]_y}$	Choice of working fluid, estimation of maximum heat flux
Goncharov-Kolesnikov (*Go*)	This criterion comes from the specific conditions of the amount of working fluid [6]. This relation is between the LHP evaporator and compensation chamber volume and the remaining LHP volume (i.e., volumes of LHP elements: - wick, grooves, condenser, vapor and liquid lines): $\left[A_1(V_l+V_v+V_c)-A_2V_w+A_3V_{vg}\right]/V_{cc}$	Condition of LHP design. Criteria of LHP start-up and operation
	Phenomenal	
Bond (*Bo*)	Quantitatively compares the relative effects of gravity and surface tension forces: $\frac{(\rho_l-\rho_v)gd^2}{\sigma}$	Determination of gravitational effects on LHP operation
Reynolds (*Re*)	Ratio of characteristic times of momentum diffusion and advection (Convection= advection + diffusion): $\frac{\rho v d}{\mu}$	Determination of flow regimes in the LHP elements
Kossovich (*Ko*)	Gives the dependence between the quantities of heat expended in evaporating the liquid and in heating the wet body [7]: $\frac{h_{fg}\dot{m}}{q_{leak}}$	Estimation of heat leak effect across LHP wick
Peclet (*Pe*)	Represents the relative magnitude of convective to conductive heat transfer: $\frac{v\rho c_p}{\lambda/\delta_w}$	Determination of primary heat transfer rate in the evaporator wick
Knudsen (*Kn*)	Ratio of mean free path to the characteristic length of the passage: λ_{free}/d	Classification for fluids deviating from continuum behavior
	Limiting	
Capillary (*Ca*)	For LHP evaporator application, *Ca* is the ratio between the liquid velocity associated with the heat transport rate (evaporation) and the speed of the capillary rise: $\frac{v}{v_{cap}}$	Dimensionless presentation of the LHP evaporator capillary limit

Boiling (*Bl*)	For LHP case, the ratio between the liquid temperature in the evaporator core and the superheat temperature corresponding to boiling	$\frac{T_{ev,core}}{T_{sup}}$	Restriction of LHP operation due to boiling (evaporator)
Viscous (*Vi*)	Dimensionless viscous limit is proportional to the vapor pressure drop in the wick divided by saturation pressure of vapor at the operational temperature	$\frac{\Delta P_v}{P_v}$	Limit of LHP operation due to vapor viscous losses in the wick
Mach (*Ma*)	Ratio between vapor velocity for chosen heat load and velocity of sound	v/v_{sound}	LHP sonic limitation

Thus, LHP criteria can be formally divided into three groups (according to criteria sources: heat and mass transfer theory, heat pipe theory, and experiment): phenomenal, limiting, and functional. The criteria from the functional group are used at the stage of choosing a working fluid, determining the amount of required fluid charge, mass-size-geometric restrictions, etc. Distinctive features of this group are based mostly on experimental characteristics and their relation to a particular class of heat pipes. Phenomenal criteria reflect the physical phenomena in heat pipes and allow for conclusions to be drawn about characteristic heat and mass transfer processes and the influences and magnitude of different forces. In accordance with common practice in heat pipes, several operating limits must be examined, including the Capillary, Viscous, Sonic, Entrainment, and Boiling limits [4]. Using these limitations as a foundation, it is possible to determine corresponding dimensionless criteria. This division is relative, however, and some numbers can belong to two groups (Fig. 5). Where the Mach (sonic limit), Weber (entrainment limit), and Capillary (capillary limit) are good examples. Furthermore, the separation of the vapor and liquid lines easily leads to the

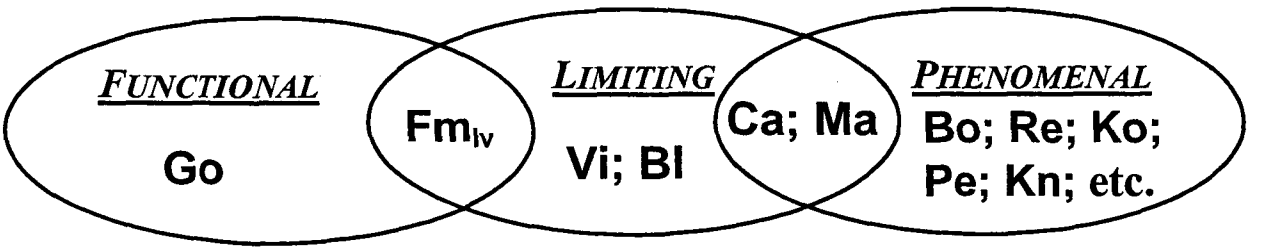

Fig. 5 Three groups of LHP operational criteria.

elimination of the entrainment limitation. In addition, some criteria such as the viscous and boiling limitations carry different meanings in the LHP case.

In Table 3, several dimensionless criteria were noted for detailed consideration. This list is, of course, incomplete. Many different dimensionless parameters, such as the set of 18 numbers introducted and investigated by Delil [1], can also be introduced for heat pipe analysis. The distinguishing feature of

our set, however, is the strong physical basis and practical significance of each criterion. In the following paragraphs, discussion focuses on selected criteria in detail.

Functional LHP Criteria

Fluid Selection Criterion

One of the first steps in heat pipe design is the selection of the working fluid. After the selection of fluids under the desired operational temperature ranges (at this stage, the lowest non-operational temperature conditions of the heat pipe [cold case] should also be taken into account because of the complex and sometimes unpredictable character of loop heat pipe start-up from the frozen state) the assorted group of fluids should be tested using several different criteria, including: wick and heat pipe body material compatibility, safety (toxicity, fire and explosive risk), chemical stability, reasonable saturated vapor pressure values in the operational temperature range, and resistance to ionizing radiation (especially for space applications). The most important criterion, however, is the combination of the physical properties of the fluid, e.g., latent heat of vaporization, surface tension, vapor and liquid densities, vapor and liquid viscosities, and contact angle on the wick material. For "classical" heat pipes, the greatest pressure loss generally occurs in the wick (liquid laminar flow). The figure of merit suggested by Chi [8] is a liquid based criteria where:

$$Fm_l = \rho h_{fg} \sigma / \mu_l \tag{39}$$

The figure of merit for popular heat pipe working fluids as a function of temperature is presented in Fig. 6.

In many cases, the pressure drop in the LHP vapor line may be considerably higher than the wick pressure drop. Dunbar and Cadell [9] proposed using another criterion in LHP based on the suggestion that liquid pressure drops could be neglected when compared with vapor pressure drops, assuming turbulent flow in the vapor line:

$$Fm_v = \rho_v h_{fg}^{1.75} \sigma / \mu_v^{0.25} \tag{40}$$

However, the dominant character of vapor pressure losses in the total LHP pressure balance is debatable. In many practical applications, the pressure drop across the evaporator wick is larger or has the same order of magnitude as that in the vapor line. If the distance between the heat sink and heat source is reduced and/or the wick thickness is increased and/or the effective pore diameter is reduced, then the wick pressure losses will increase. Thus, it is difficult to make a correct selection of the working fluid

using either of the two figures of merit if the geometrical characteristics of the LHP are not taken into account. The governing pressure balance for an LHP, assuming turbulent flow in vapor line and laminar flow in the wick and liquid line, can be written in the form [10]:

$$\frac{4\sigma\cos(\theta)}{d_p} = f_{turb}\frac{\rho_v v_v^{\,2}}{2d_v}l_{lhp} + \frac{16v_w\mu_l}{d_p^{\,2}}(d_2 - d_1) + \frac{32v_l\mu_l}{d_l^{\,2}}l_{lhp} \qquad (41)$$

The velocities of the working fluid in the wick v_w, vapor v_v, and liquid v_l lines can be determined by:

$$v_w = \int_{d_1/2}^{d_2/2} v_w(r)\,rdr \Big/ \int_{d_1/2}^{d_2/2} rdr = 2q \Big/ \left[\pi h_{fg}\rho_l\varepsilon L_w(d_2 + d_1)\right] \qquad (42)$$

$$v_l = 4q/\pi\rho_l h_{fg} d_l^{\,2} \qquad v_v = 4q/\pi\rho_v h_{fg} d_v^{\,2} \qquad (43)$$

Pressure losses in the evaporator vapor grooves, compensation chamber, and condenser that result from the relatively small length of each are neglected. Because the friction factor in the area of fully developed turbulent flow is practically constant, a second order equation is obtained for the maximum heat flux q. The idea of applying this type of quadratic equation for "classical" heat pipes having wicks of uniform pore size can also be found in reference [11].

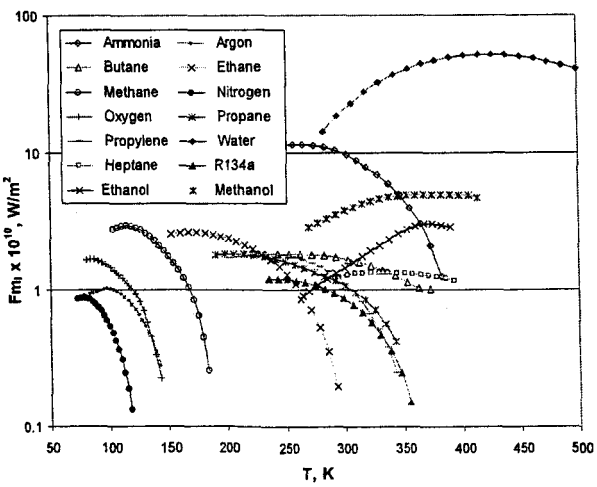

Fig. 6 Figure of merit (liquid-based) for different fluids

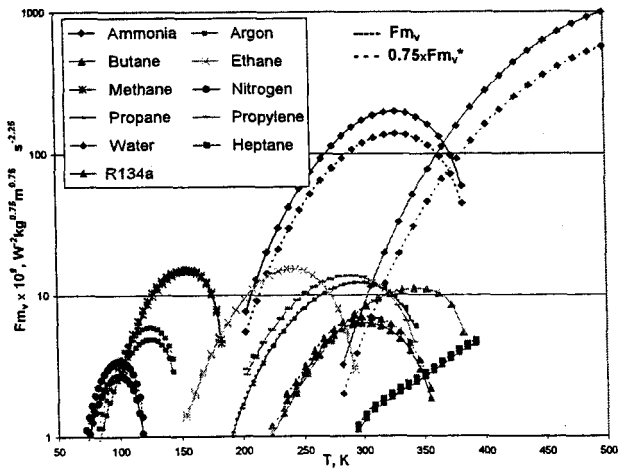

Fig. 7 Comparison of Fm_v^* and Fm_v figures of merit for different working fluids

As taken from the general Moody diagram found in almost every fluid mechanics text, the dimensionless friction factor is constant and relative roughness lies in the range of 0.07 - 0.007 for the

practical area of LHP design. The Colebroock equation for the friction factor in the fully turbulent region ($Re \to \infty$) reduces to:

$$f_{turb} = 0.25 \log\left(\varepsilon_t / 3.7 d_v\right)^{-2} \tag{44}$$

The resulting quadratic equation has only one positive root, resulting in the vapor-liquid figure of merit for the working fluid selection (and, simultaneously, a criterion for the estimation of the maximum heat flux) in loop heat pipes:

$$Fm_w = \frac{\left((2.55Kl)^2 + 0.2Kv\right)^{0.5} - 2.55Kl}{0.1Kv} \tag{45}$$

$$Kl = \frac{Geo_l}{Fm_l^*} \qquad Kv = \frac{Geo_v}{Fm_v^*} \tag{45a}$$

$$Geo_l = \frac{(d_2 - d_1)}{(d_2 + d_1)\varepsilon^{0.67} l_w d_p} + \frac{4 d_p l_{lhp}}{d_l^4} \qquad Geo_v = \frac{d_p l_{lhp}}{\log\left(\varepsilon_t / 3.7 d_v\right)^2 d_v^5} \tag{45b}$$

$$Fm_l^* = Fm_v \cos(\theta) \qquad Fm_v^* = \rho_v h_{fg}^2 \sigma \cos(\theta)$$

This criterion depends on the geometry of the design problem (l_{lhp} can be considered as the distance between heat source and sink), the geometry and physical characteristics of the wick, the latent heat of vaporization, surface tension, vapor and liquid densities, liquid viscosity, and the contact angle with the wick material. Because the contact angle (for an LHP, it is the apparent contact angle of an inverted, evaporating meniscus) is not a tabulated parameter and because it is difficult to find the values for different combinations of wick material and working fluid in the literature, the contact angle is assumed equal to zero (which is the usual but not obvious selection with heat pipe researchers and engineers). As a result, $Fm_l^* = Fm_l$ and $Fm_v^* = \rho_v h_{fg} \sigma$. The modified Fm_v^* number does not depend on vapor viscosity as in the original criterion suggested by Dunbar and Cadell, as the dependence on vapor viscosity is very weak and can be ignored. It is clear from Fig. 7 that the fluid-properties groups Fm_v^* and Fm_v have the same characteristic dependence on temperature for all fluids. Moreover, $Fm_v \approx 0.75\, Fm_v^*$ for all fluids except ammonia and water. In a general case, if a designer is sure that the vapor line pressure losses are dominant, it is preferable to use the Fm_v^* figure of merit for fluid selection.

If the wick permeability, K, is known, the pressure drop in the wick can be determined from the Darcy filtration law, causing the geometrical parameter of the liquid flow to be:

$$Geo_l = \frac{d_p \ln(d_2/d_1)}{64 l_w K} + \frac{4 d_p l_{lhp}}{d_l^4}; \qquad (46)$$

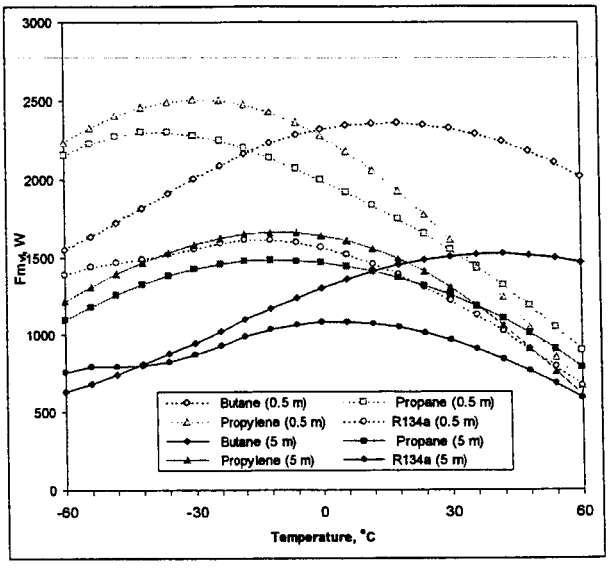

Fig. 8 Figure of merit Fm_{vl} for different LHP lengths (l_{lhp} =0.5, 5 m, d_p=1 μm, δ_w=4 mm) versus operational temperature.

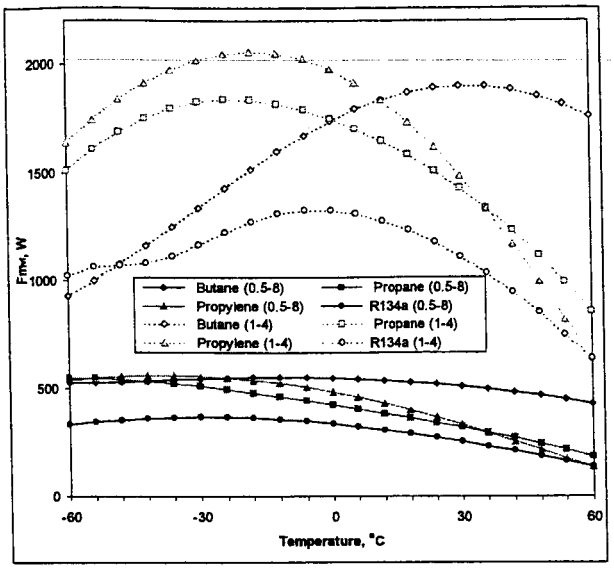

Fig. 9 Figure of merit Fm_{vl} for different wick dimensions (l_{lhp} =2 m, d_p=0.5, 1 μm, δ_w=4, 8 mm) versus operational temperature.

The importance of the geometrical characteristics of an LHP and the wick regarding the fluid selection process can be demonstrated by the following example. According to Dunbar and Cadell, the best liquid in the range –60 to 60 °C is propylene (after ammonia, of course), but, according to the Chi criterion, butane is the better liquid. As can be seen from Figs. 8 and 9, the butane advantage over propylene increases with the LHP length increasing, the wick effective diameter decreasing, and the wick thickness increasing. Also, the two graphs above reflect the general tendency of the maximum heat flux to increase with the reduction of the liquid and vapor lines lengths, the lessening of wick thickness, and the increase in the effective pore diameter of the wick. The following geometric parameters of the evaporator were chosen for the calculations: d_1=8, 16 mm, d_1=24 mm, l_w=100 mm (length of evaporator active zone), d_v=6 mm, d_l=4 mm d_p=0.5, 1 μm, ε=0.7, ε_t=0.002 mm (stainless steel) l_{lhp} =0.5, 2, 5 m. The obtained range of maximum heat loads (0.5 – 2.5 kW) for assorted liquids and for an LHP with the given geometry is close to experimental levels and supports the presented approach and criteria for fluid selection.

Thus, existing relations between surface tension, latent heat, viscosity, and density of working fluids cannot be used in the general case of LHP design. The specific LHP geometry, however, is presented in

the new Fm_{lv} figure of merit. This figure of merit allows for the drawing of more accurate conclusions about the suitability of working fluids for given LHP operational conditions.

Goncharov-Kolesnikov Criterion

A very important characteristic of every heat pipe or thermosyphon is the charging amount of working fluid. The amount of fluid for "classical" heat pipes is usually calculated using the relation:

$$M = F_o\left(V_w\rho_l + V_v\rho_v\right) \tag{47}$$

The term F_o is an optimization factor that is determined experimentally and usually varies in the range from 0.9 to 1.5. In the case of an LHP, however, this relation is not valid.

The second functional criterion comes from two specific conditions in the charge amount of working fluid in an LHP. First, liquid should be left in the compensation chamber (CC) when the rest of loop is completely flooded under cold cases (condition of the LHP before start-up). Second, an amount of vapor space should be available in the compensation chamber when the condenser is fully utilized under a hot case [12]:

$$\begin{aligned} M &= \rho_{l_{cold}}\left(V_{loop} + \beta V_{cc}\right) + \rho_{v_{cold}}\left(1-\beta\right)V_{cc} \\ M &= \rho_{l_{hot}}\left(V_l + V_w + \left(1-\alpha\right)V_{cc}\right) + \rho_{v_{hot}}\left(V_{gr} + V_v + V_c + \alpha V_{cc}\right) \end{aligned} \tag{48}$$

If the relation between the volume of liquid line and volumes of the condenser and vapor lines is introduced: $k=V_{liq}/(V_{con}+V_{vap})$, then the functional criteria between the compensation chamber volume and the volumes of other LHP components can be derived as follows:

$$\begin{aligned} Go &= \left(A_1\left[V_c + V_l + V_v\right] - A_2V_w + A_3V_{gr}\right)/V_{cc} \le 1 \\ A_1 &= A\left(\rho_{l_{cold}} - \left(k\rho_{l_{hot}} + \rho_{v_{hot}}\right)/\left(1+k\right)\right) \qquad A_2 = A\left(\rho_{l_{hot}} - \rho_{l_{cold}}\right) \\ A_3 &= A\left(\rho_{l_{cold}} - \rho_{v_{hot}}\right) \quad A = \left[\rho_{l_{hot}} - \rho_{v_{cold}} - \beta\left(\rho_{l_{cold}} - \rho_{v_{cold}}\right) - \alpha\left(\rho_{l_{hot}} - \rho_{v_{hot}}\right)\right]^{-1} \end{aligned} \tag{49}$$

This relation is an expanded form of the LHP design criterion presented by Goncharov and Kolesnikov [6]. It should be mentioned, though, that Gerasimov et al.[13] first described this LHP charging condition in a qualitative form in 1976. In many cases of LHP design, the length of the liquid line is equal to that of the vapor line. Neglecting the volume of the condenser ($V_l=kV_v$), the coefficient k is equal $(d_l/d_v)^2$.

The dependence of the compensation chamber volume on operational temperature for different LHP lengths and the fractions of the compensation chamber occupied by liquid at the minimum temperature and void fraction are shown in Fig. 10. Calculations are made for ammonia as the working fluid, and the temperature of the cold case was –70 °C. The geometric parameters were d_{gr}=1 mm, n=20, d_1=10 mm,

l_{lhp} =0.5, 5 m. All other data are the same as indicated for the Fm_{vl} comparison. It is obvious that the volume of the compensation chamber increases with an increasing LHP length, increasing operational temperature, and increasing coefficients α and β. The influence of β on compensation chamber volume is stronger than the influence of α. As a rule, this coefficient is varied in the range from 0.05 - 0.4, but α and β should be as small as possible in order to minimize the LHP total mass.

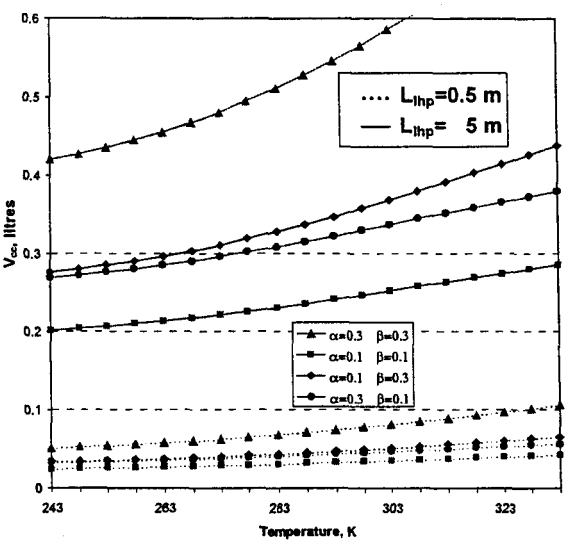

Fig. 10 Compensation chamber volume for different LHP (ammonia) lengths.

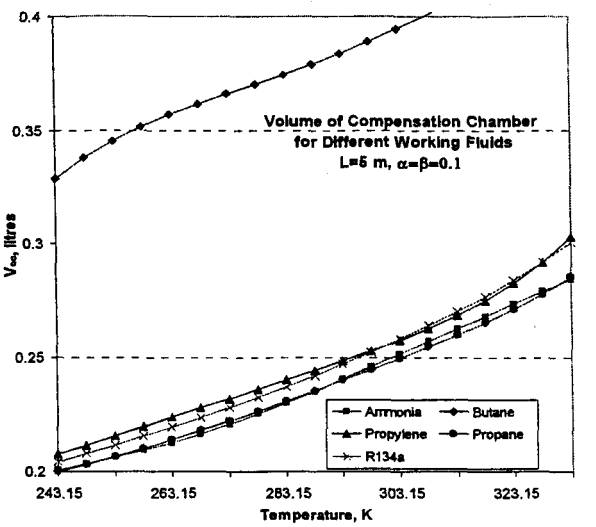

Fig. 11 Compensation chamber volume for different working fluids.

From the results of the calculated compensation chambers volumes for different working fluids (Fig. 11), it is possible to draw the conclusion that, if the LHP is designed for propylene, this LHP can be recharged by ammonia, R134a, or propane and will be able to start-up and operate. On the other hand, the butane LHP requires a larger compensation chamber volume in comparison with the ammonia LHP (1.5 – 2.5 times).

Phenomenal LHP Criteria

An enormous number of dimensionless groups can be found in heat and mass transfer literature. Based on the main physical phenomena that are presented in the LHP of Fig. 12, some of the more valuable and interesting numbers were selected and are discussed in this section of the report.

Bond Number

The behavior of the liquid/vapor boundary surface meniscus in the LHP evaporator microporous capillary structure has a critical significance for the start-up and operation of LHP devices. The nature of evaporated, "inverted," menisci behavior in the LHP evaporator is very complex. According to the

modern conception of heat transfer for liquid/vapor phase change surface during evaporation [14], the meniscus can be divided into the following sections:

1. Adsorbed film. Monolayer to 0.05×10^{-3} mm; Evaporation is absent (liquid is overheated). Disjoining pressure is dominant [15];
2. Inner intrinsic region up to 0.001-0.1 mm; Extremely high evaporation. Disjoining pressure has the same order as capillary pressure;
3. Bulk meniscus, region I up to 1 - 10 mm; Heat transfer by thermal conduction. Heat transfer coefficient drops up to minimum value [16];
4. Bulk meniscus, region II; Heat transfer by natural convection-buoyancy. Heat transfer rises up to constant value.

Marangoni surface convection and meniscus oscillation (at film thicknesses less than 1 mm) as a result of interaction among thermocapillarity, evaporation, and the liquid inertia feeding the meniscus are additional effects that can influence meniscus behavior during phase change heat transfer. The pulsation of the contact line amplifies with increasing heat flux. As can be seen, characteristic scales determine the significance and magnitude of different effects and forces.

Under terrestrial conditions, the gravitational force field has a strong influence on LHP working parameters. The magnifitude of this influence relative to surface tension forces, which create a pressure difference across the two-phase boundary, can be estimated with the help of the Bond number.

This number allows for the drawing of a conclusion that takes gravity into account in LHP modeling. Also, the characteristic size d_{char} of the wick pores, vapor collecting grooves, and the LHP vapor/liquid lines effective diameters can be investigated. A Bo of unity indicates that the capillary and gravitational effects are of the same order of magnitude. The name of the characteristic size corresponding to $Bo=1$ is Bond length. The decrease of Bo indicates that the surface forces become dominant. Microgravity usually is defined as $Bo < 10^{-3}$. In the region $10^{-3} < Bo < 10^{3}$, both gravity and surface tension effects should be taken into account. It is possible to introduce the parameter of Microgravity Bond length for the condition $Bo < 10^{-3}$.

$$d_{mbl} = \sqrt{0.001\sigma / g(\rho_l - \rho_v)} \tag{50}$$

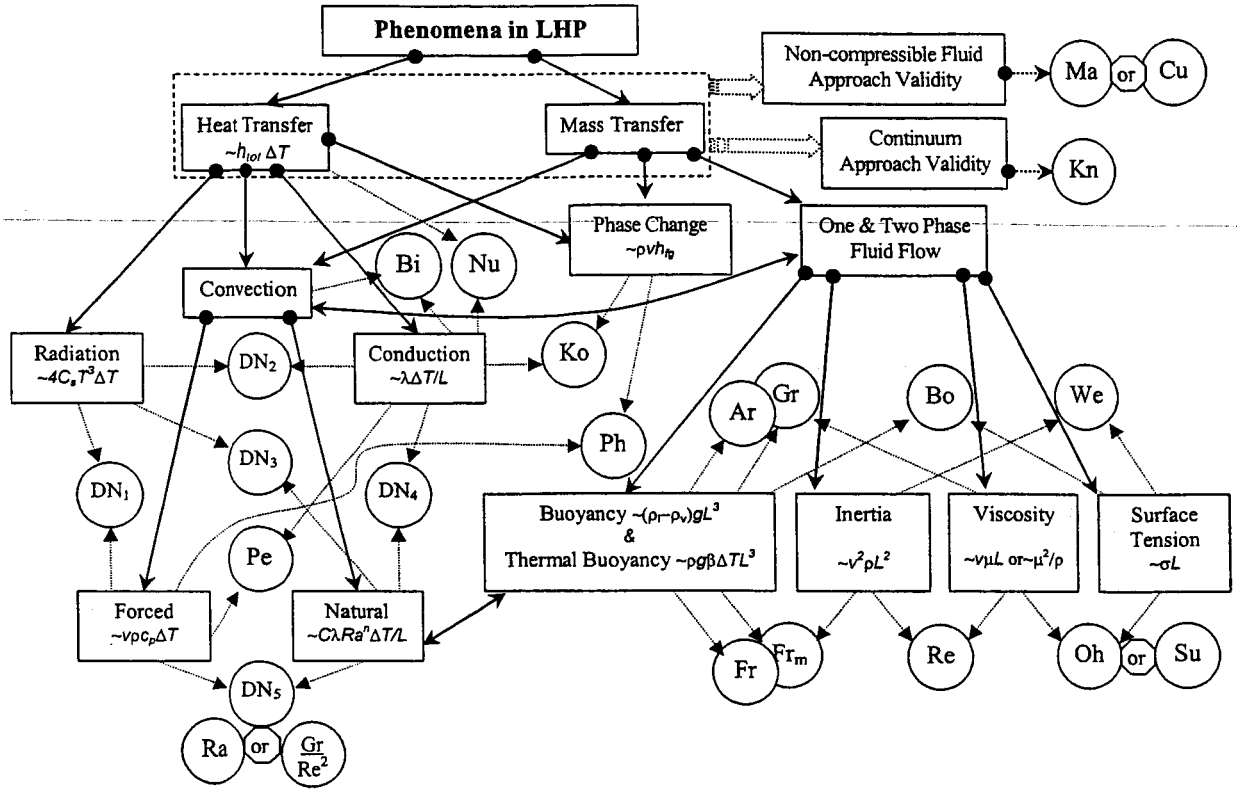

Fig. 12. Phenomena in the LHP and dimensionless groups.

In Table 2, Bond lengths and Microgravity Bond lengths for popular LHP working fluids for temperatures from cryogenics to ambient are presented. As a rule, the d_{mbl} lies in the dimension diapason 10÷100 μm. This diapason is very common for the effective pore diameters of LHP evaporator wicks. Consequently, the value of *Bo* is an extremely important characteristic for LHP design and modeling. Put simply, if the wick effective pore diameter is less then 10 μm, the condition of microgravity realized in the LHP wick and gravity forces do not need to be taken into account. The dependences of the Bond number on the operational temperature for ammonia, propane, butane, propylene, and R134A are shown in Fig. 13 (d = 1 μm). *Bo* is increasing for all fluids as the temperature increases.

Reynolds Number

As a parameter that takes into account the fluid density, viscosity, and velocity, as well as the dimensions of the channel for heat and mass transfer theory and devices, the Reynolds number is extraordinarily significant. Though Reynolds presented this number 120 years ago [17], it is unimaginable to perform any flow analysis and calculations without referring to this number.

Table 4 - Bond lengths and Microgravity Bond lengths for popular LHP working fluids and for different operational temperatures.

Working Fluid	Bond length, mm (Microgravity Bond length, μm)		
	–160°C	**–60°C**	**40°C**
Ammonia	-	2.40 (75.9)	1.75 (55.3)
Argon	0.78 (24.7)		-
Butane	-	1.89 (59.8)	1.43 (45.2)
Ethane	-	1.53 (48.4)	-
Ethanol	-	-	1.67 (52.8)
Heptane	-	-	1.69 (53.4)
Methane	1.81 (57.2)	-	-
Methanol	-	-	1.66 (52.5)
Nitrogen	0.62 (19.6)	-	-
Oxygen	0.92 (21.9)	-	-
Propane	-	1.75 (55.3)	1.08 (34.2)
Propylene	-	1.74 (55.0)	1.05 (33.2)
R134a	-	1.20 (38.0)	0.75 (23.7)
Water	-	-	2.69 (85.1)

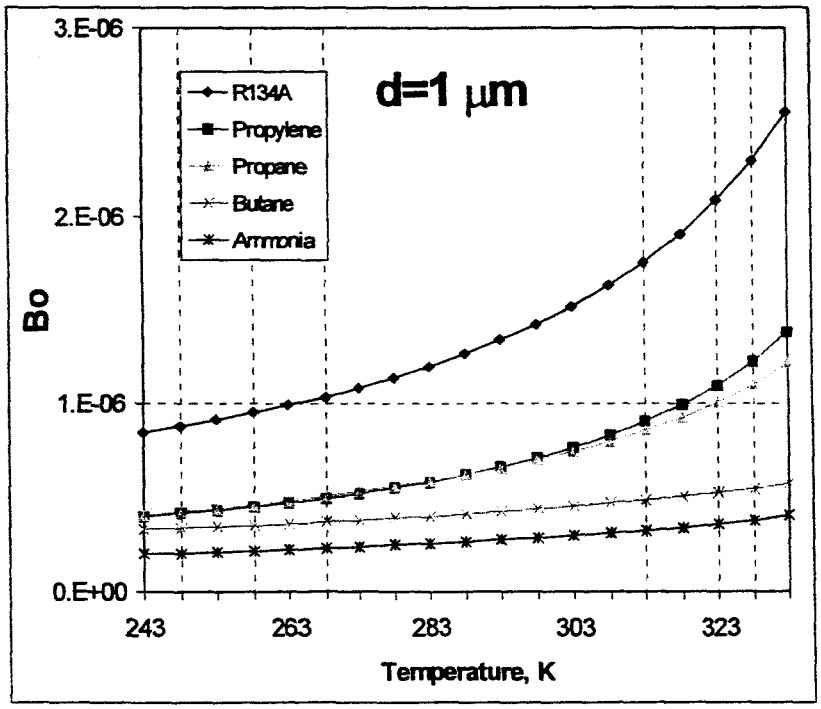

Fig. 13 Bond number vs operational temperature for different fluids

An estimate of the liquid velocity from the applied heat rate to the evaporator (while neglecting heat leak into the LHP evaporator core) can be found by:

$$v = q_{ev} / \rho h_{fg} \qquad \text{where} \qquad q_{ev} = Q_{ev} / \varepsilon^{2/3} \pi d_2 l_{ev} \qquad (51)$$

The LHP evaporator model is presented in Fig. 2 (the compensation chamber is not shown). The capillary wick is modeled as a bundle of cylindrical parallel capillaries of fixed diameter that is equal to the effective pore diameter of the wick d_p.

As a rule, the liquid or vapor flow regimes in the evaporator capillary wick are very far from turbulent ($Re << 2300$). For channels only several or tens of microns across, the diminutive conduits lead to very small Reynolds numbers (less than unity) even for vapor media and very high heat loads.

Peclet and Kossovich Numbers

The modeling of the loop heat pipe (LHP) evaporator is commonly simplified by neglecting the effects of convective heat transfer in the evaporator wick when compared to conductive heat transfer [18,19,20]. Investigators typically use Fourier's Law with the effective thermal conductivity of the wick as a basic parameter for describing heat transfer phenomenon in the evaporator and for determining the amount of heat leak from the high-pressure side of the wick to the low-pressure side.

The basis for the assumption of neglecting the convective effects is not obvious, however, as the wick represents a convective-diffusion problem and not, systematically, a diffusion (conduction) problem. Because it represents the relative magnitude of convective to conductive heat transfer with moving liquids, the Peclet number becomes an interesting parameter to use in estimating the convective part of the entire heat transfer across the wick.

Typically, the overall heat leak across the wick is not more then several percent of the overall heat input for a traditional LHP with middle to high heat inputs. The dimensionless Kossovich number [7] gives the dependence between the quantities of heat expended in evaporating liquid and in heating the wet body. In the heat pipe case, this number gives the dependence between the heat flux coming out of the wick in vapor form and the heat flux coming into the evaporator core from heat conduction, convection, and radiation. By neglecting the convection and radiation terms (for comparative purposes), and by defining the inner heat rate (leak) as conductive only:

$$q_{leak} = \frac{\lambda_{eff} \Delta T}{ln(d_2/d_1)} \qquad (52)$$

The evaporating rate can then be defined as the difference between the total heat load and the amount of conductive heat coming into the wick. The Kossovich number is consequently given as:

$$Ko = \frac{q_{ev} - q_{leak}}{q_{leak}} \tag{53}$$

As noted, this calculation does not take into account the fluid motion inside the wick. If $Pe > 0.01$, the real Ko number will be greater (and the real heat leak in the evaporator core will be less). Practically, Ko for an LHP evaporator can also be interpreted as a Kirpichev or Jacobs number by physical meaning. From analysis of the Kossovich number, it is possible to draw conclusions about the validity of Eq. (51) for Peclet number calculation.

With growth of the wick-skeleton thermal conductance, the influence of liquid thermal conductivity on the Peclet number decreases. The role of convection, however, increases with increases in operational temperature and heat input.

From the Peclet number, the necessity of including convective effects can be determined. In cases where the problem is a convective-diffusive system, the governing equation for the temperature field can be estimated from the solution to the general energy equation. Solutions using a pseudo-convective coefficient in order to reduce the energy equation and thereby allow for easier analytical solutions have been presented in [2].

Using basic, non-dimensional Kossovich and Peclet numbers, the modeling of the LHP evaporator based on the assumption that the process of heat transfer into the wick core (heat leak) requires the conduction approach can be shown to be incorrect in the majority of practical cases. In the continuous desire to reduce the effective thermal conductivity of the wick, a limit exists where the thermal conductivity no longer is the dominant factor. For example, in Teflon wicks, the convective effects are more important than the conductive effects because of the small wick-skeleton thermal conductivity as compared with metallic wicks.

Capillary Number

Capillary action in the wick is the main distinguishing feature of heat pipes as heat transfer devices. Consequently, the phenomenon of capillarity is a key characteristic for the LHP, and all dimensionless complexes inclusive of surface tension and contact angle (two main characteristics of capillarity phenomenon) are very important. By definition, the Capillary number is the ratio between viscous stresses and interfacial tension. In the case of LHP, we can give a "special edition" of the Capillary number as an evaporator capillary limitation for heat pipe operation. The LHP can operate until the velocity of capillary rise is equal to or more than the velocity of the evaporation from the phase boundary surface (heat rate-based mass flow). Due to the laminar regime of the liquid flow (Poiseulle approach) in the wick (see above Reynolds number):

$$Ca = \frac{v\mu}{\sigma\cos(\theta)}\frac{4(d_2 - d_1)}{d_p} \qquad (54)$$

This dimensionless parameter can also help to estimate the significance of the contact angle value. As mentioned above (Bond number), in the general case, the contact angle is not a constant but is an apparent contact angle and is a function of the heat rate.

The operation of an ammonia LHP does not depend strongly on the contact angle at relatively small heat rates. With rise of heat load, however, this dependence can be critical and can lead to failure of LHP operation. This critical dependence is clear from an analysis of the curves derived from plotting Capillary numbers as a function of operational temperature for different heat rates and contact angle values (Fig. 14). The following geometric parameters of the evaporator were chosen: d_2=24 mm, d_{gr}=2 mm, l_{ev}=100 mm, d_p=1 μm, ε=0.7.

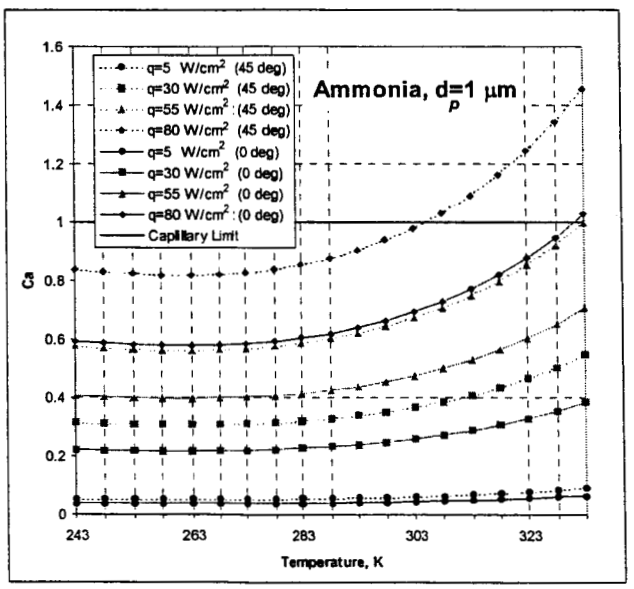

Fig. 14 Ammonia Capillary Number for different heat rates and contact angle values as a function of operational temperature

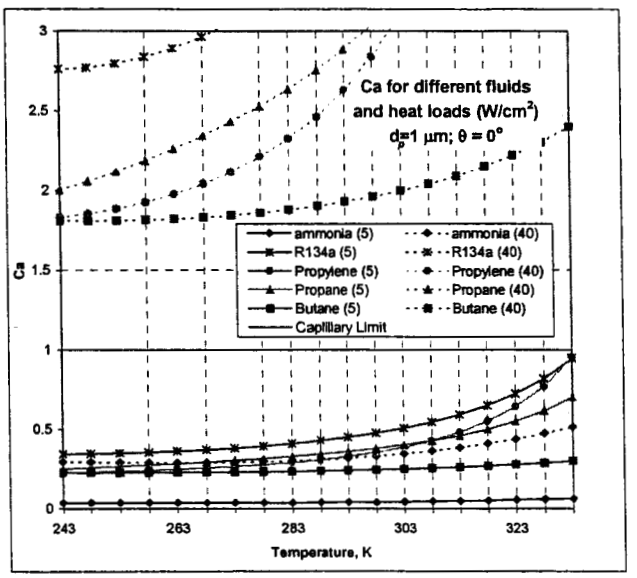

Fig. 15 Capillary Numbers of several heat pipe working fluids for different heat rates as a function of operational temperature

It is impossible not to admit that an "understanding of the heat transfer characteristics of an evaporating extended meniscus is of central importance to the design" of the LHP [21]. Currently, though, it seems "there are not any theoretical and experimental bases to estimate contact angle values" [22]. In actuality, however, the last assertion is not quite true. Many researchers have tried to predict and measure contact angles. But we are still at the beginning of the process. The theory of apparent contact angle for non-polar liquids is well developed by P.C.Wayner Jr. with co-workers. The augmented Young-Laplace

model of an evaporating meniscus for capillary pressure drop determination is the starting point for present theoretical conceptions [21]:

$$P_c = -\frac{2\sigma}{r} + \Pi(\delta) \tag{55}$$

where $\Pi(\delta)$ is the disjoining pressure as a function of the thickness of the liquid film δ.

If the liquid film dependence on coordinate y along the capillary channel is known, the apparent contact angle will be $\theta_a = \arctan(d\delta/dy)$. For non-polar liquids, the disjoining pressure can be easily determined [23]:

$$\Pi = -\frac{A}{\delta^3} \tag{56}$$

where A is the Hamaker constant.

Unfortunately, many LHP working agents are polar liquids with a high dipole momentum: water (1.9 D), ammonia (1.5 D), propylene (0.4 D), R134a (2.1 D), ethanol (1.9 D), methanol (1.9 D). Even using this relation for ammonia [24] (the equity of this approach is very debatable) gives the strong dependence of the apparent contact angle on superheat drop between temperatures of the wall and of the interface. The highest superheat values occur at the highest contact angle values (up to 30°) and thereby lessen the heat rate limit according to Ca number limitation. In reference [25], the authors used Eq. (56) for describing water meniscus evaporation. Water, however, belongs to the polar liquids as well. As a result, not only should the Van der Waals forces be taken into account, electrostatic forces should also be taken into account. One other approach often encountered in the literature [26, 27] is the calculation of the disjoining pressure from the empirical equation:

$$\Pi = \rho_l R_g T_s \left[1.5336 \left(\delta / 3.3 \right)^{0.0243} \right] \tag{57}$$

This formula, however, came from an experimental relation obtained by Deryagin and Zorin in 1957 [28] for water film on a glass surface for a very narrow temperature range (4-15°C). Traditional heat pipe wick materials are metals or polymers. Any extension of Eq. (57) to other materials and temperature diapasons should be thoroughly argued.

The maximum heat rate has a strong dependence on the apparent contact angle. It is therefore very important to have a good model of vapor/solid/liquid contact region for correct LHP operation description. The suggestion that $\theta = 0°$ can lead to a serious overestimation of heat pipe working parameters.

Ammonia's unique physical properties allow LHP to be charged with ammonia in order to operate at much higher heat loads then LHP with any other working agent in the temperature range from –30 to 60 °C (Fig. 15). Almost no fluids other than ammonia can be used (for the given structural and geometrical parameters of the evaporator wick) for transfer heat rates up to 40 W/cm^2.

Knudsen Number

The vapor zone can penetrate relatively deeply into the capillary wick before the operation of an LHP system fails as a result of the viscous limit. It is important to estimate the character of vapor flow in the wick for correct LHP modeling. The key criterion for this estimation is the Knudsen number, whereas the characteristic flow dimension for our case is the effective pore diameter d_p of the LHP evaporator wick.

According to definition [29], the Knudsen number, in particular flows, determines the degree of flow rarefaction and the degree of validity of the continuum approach:

- Euler equation (neglect molecular diffusion) $Kn \to 0\ (Re \to \infty)$
- Navier-Stokes equations with no-slip boundary conditions $Kn < 10^{-3}$
- Navier-Stokes equations with slip boundary conditions $10^{-3} \le Kn < 10^{-1}$
- Transition regime $10^{-1} \le Kn < 10$
- Free molecule flow $Kn \ge 10$

For an ideal gas model (molecules are rigid spheres), the mean free path is related to a temperature and pressure:

$$\lambda_{free} = \frac{1}{\sqrt{2}\pi n d_w^{\,2}} = \frac{kT}{\sqrt{2}\pi p d_w^{\,2}} \tag{58}$$

Molecular, or Van der Waals, diameter is connected with vapor density. Consequently, [30]:

$$\lambda_{free} = \frac{\mu\sqrt{\pi}}{\rho\sqrt{2R_g T_v}} \tag{59}$$

It should be mentioned that Eq. (59) is valid only for vapor flow. Unfortunately, at present, despite the very quickly growing volume of experimental data, there is no special parameter for the characteristic classification of liquid flows in micro-channels, as there is for gas and for vapor flows. This is because the concept of a mean free path is not very useful for liquids, and the conditions under which a flow fails to be a Newton liquid flow are not well defined. Moreover, the experimental data of flow in micro-channels

are quite contradictory. For flows in micro-channels, the phenomenological approach for analyzing the data is to define an apparent viscosity μ_a calculated so that if μ_a were used in the traditional, no-slip Navier–Stokes equations, instead of the liquid viscosity μ_l, the results would be in agreement with experimental observations. One researcher reports that μ_a is increasing as the micro-channel diameter decreases, while another reports that μ_a dramatically decreases relative to the macro value of viscosity. A third tells that $\mu_a=\mu_l$ for thin-film flows as long as the film thickness exceeds 10 molecular layers. A very good overview of the literature written on this question was made by Mohamed Gad-el-Hak [29]. Although the majority of the experimental results testify to validate Navier-Stokes equations with a no-slip boundary conditions approach (macroscale continuum theory) to liquid microflow modeling up to a channel diameter of 0.1-1 μm, additional experimental and theoretical research efforts are required.

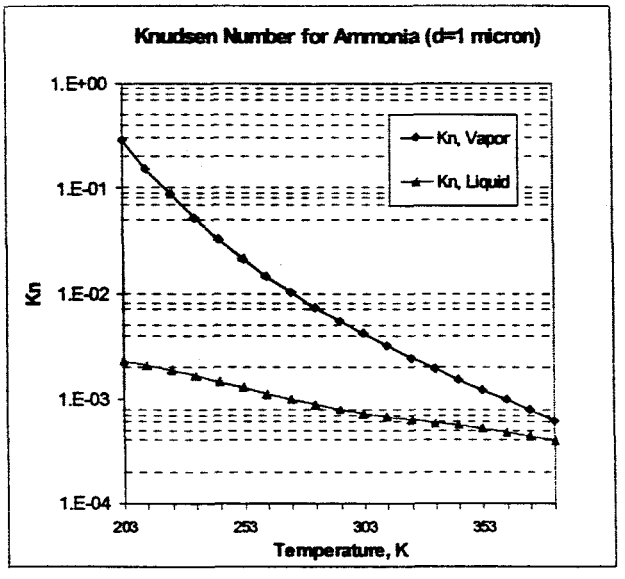

Fig. 16 The dependence of the Knudsen Number for ammonia on temperature.

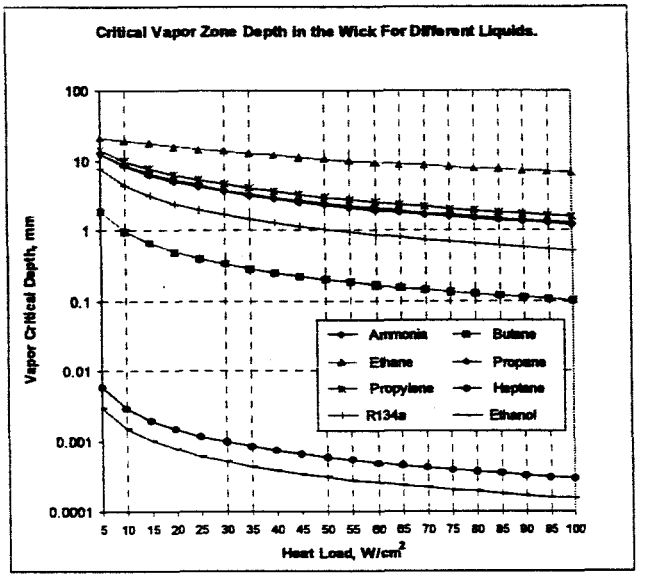

Fig. 17 Critical vapor zone depth in the wick for different LHP working fluids as a function of heat load (operational temperature is 20°C, dp=1 mm).

In Fig. 16, the Knudsen number dependence on the working temperature of ammonia LHP for an effective pore wick diameter of 1 μm is presented. The vapor flow inside the wick should be considered as a slip flow in almost all the working ranges of ammonia (except for very high and very low temperatures) for the chosen characteristic flow dimension. In addition, *Kn* was determined from Eq. (59) for liquid flow for illustrative purposes.

Limiting LHP Criteria

Viscous Criterion

In the case of the same specific conditions for ordinary heat pipes and thermosyphons (very low operational temperature for the given working fluid and/or an extremely long heat pipe and/or start-up from the frozen state), the vapor pressure drop between evaporator and condenser may be extremely small. If vapor viscous pressure losses are larger then the pressure gradient caused by the imposed temperature difference, flow will not be generated, and the vapor may stagnate. This no-flow or extremely low-flow condition in the vapor portion of heat pipe is referred to as the viscous limitation [4].

For the LHP, this limit has a different, special meaning. During LHP operation, the boundary surface between vapor and liquid zones is presented inside the capillary wick. This surface is moved deeper into the wick with the increase of the heat load (see, for example [18]). Based on what has already been assumed in this report, namely that the LHP evaporator capillary wick model is a series of independent cylindrical channels with a radius equal to the effective pore radius of the capillary structure, it is possible to estimate the maximal depth of the vapor-liquid boundary from the adaptation of the classical dimensionless viscous limit of heat pipe operation ($\Delta P_v/P_v < 0.1$) to LHPs conditions. ΔP_v, then, is the pressure drop occurring in the vapor phase inside the wick, and P_v is the saturated vapor pressure (corresponding to the LHP operational temperature T_v). As a rule, the Reynolds numbers for flows inside the wick are very small because of the micron sizes of pores and because flows are laminar. Thus, we can obtain the critical depth of the vapor-liquid boundary l_{cr}:

$$l_{cr} = \frac{0.1 d_p^{\,2} P_v \rho_v h_{fg}}{32 \mu_v q_{ev}} \tag{60}$$

The vapor zone critical depth dependence on heat load for different liquids is shown in Fig 17. The calculation was made for an operational temperature of 20°C and for the above-indicated geometrical parameters of the LHP evaporator. As can be seen, the critical depth decreases with the increase of the heat load. The heat load increase, however, forces the liquid to go deep into the wick and increases the probability of the operation failure of the LHP as a result of the viscous limit. The problem of phase-change boundary movement in porous structures is very important and requires more extensive experimental and theoretical investigations.

Boiling Criterion

Numerous books and papers have been dedicated to boiling and evaporation processes in heat pipes, but this problem is still quite obscure. In the "classical" heat pipe literature (see, for instance, [4, 31]), the parameter, "nucleation radius of the vapor bubbles, r_n," is introduced for boiling limitation calculations.

This parameter should be determined from specific and complicated experiments for every capillary structure, heat pipe enclosure, and working liquid. The authors [4, 8] (with reference to [32]), for estimation purposes, suggest using the very wide range of boiling limitation values from $1\times10^{-3} - 1\times10^{-5}$ in (2.54×10^{-5}-2.54×10^{-7} m). In practice, this leads to conclusions that the calculation of the boiling limitation value according to "classical" models do not have the same physical sense for microporous capillary wicks when the effective pore size is on the same order as the nucleation site. Also, most researchers suppose "a priori" that boiling in such heat pipes will never be realized because the wick dry-out due to the capillary limitation will occur first.

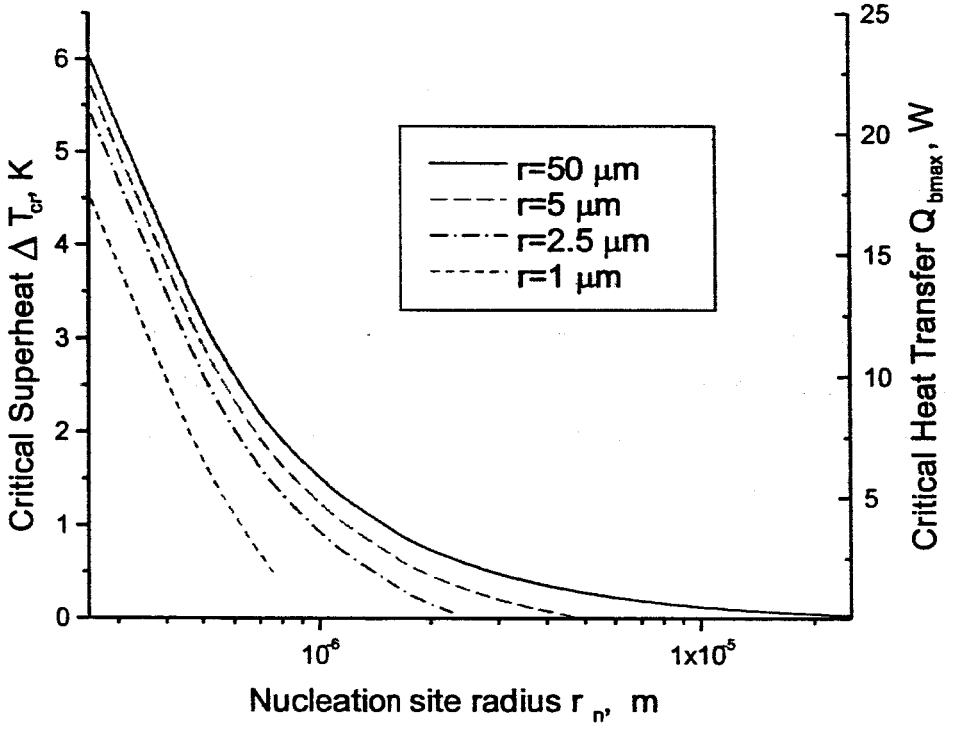

Fig. 18. Critical heat transfer and superheat temperature drop vs. nucleation site radius for different wick effective pore radiuses (ammonia LHP with nickel wick).

The following example for an ammonia LHP evaporator (operational temperature T_v = 20°C; wick material – nickel; outer wick diameter D_1 =16 mm; inner D_2=24 mm; evaporator length L_{ev} =100 mm; porosity ε =70 %; effective heat conductivity of the wick λ_{eff} =7 W/mK) for different effective pore radii of the wick (r =1 – 50 μm) is used as an illustration of the impossibility of using classical heat pipe boiling limitation theory in the case of microporous wicks. The classical equations for boiling critical superheat and for boiling heat transfer limit [8] are:

$$\Delta T_{sh} = \frac{2\sigma T_v}{h_{fg}\rho_v}\left(\frac{1}{r_n} - \frac{1}{r_p}\right) \tag{61}$$

$$Q_{bmax} = \frac{4\pi\sigma L\lambda_{eff}T_v}{h_{fg}\rho_v \ln(D_1/D_2)}\left(\frac{1}{r_n} - \frac{1}{r_p}\right) \tag{62}$$

Results of these calculations are presented in Fig. 18. Even insignificant changes of the effective radius r_n lead to serious changes of the temperature superheat and heat transfer estimations. Moreover, according to this model, the given ammonia heat pipe is incapable of transferring more than 20 – 25 W (0.27 – 0.33 W/cm^2) because of the boiling limitation. In practice, however, loop heat pipes with similar parameters can transfer up to several hundred Watts. This model is based on the suggestion that the nucleation centers are microscopic cavities with entrapped, non-condensed gases that are placed in the gap between the capillary wick and the heat pipe envelope. The presence of such cavities results in a boiling phenomenon at very small superheat levels within a few degrees of the working liquid saturation temperature. If all non-condensable gas was preliminarily removed from the system, the liquid superheat could reach up to 100 – 200 K before boiling began. This premise was experimentally confirmed by Harvey and co-workers in the 1940's [30] when Harvey deactivated surface cavities by subjecting the tested liquid and surface to high static pressures before the boiling point at atmospheric pressure measurements. The preliminary pressurized samples boiled at very high temperatures close to the superheat limit. In the experiments, Harvey et al. therefore dealt with pure liquids and pure surfaces without dissolved gases in the system. Heat pipe manufacturers always strive to minimize the non-condensable gas volume inside the heat pipe because heat pipe operation is more reliable and predictable when the amount of non-condensible gas in the heat pipe is lower. Thus, the better the heat pipe is, reaching the heat pipe boiling limitation becomes less probable. Another example confirming this conclusion is the experimental work of Barthelemy [33]. Barthelemy paid special attention to the liquid degassing (20 minutes boiling of de-mineralized, triply de-ionized triply distilled water just before filling) and to non-condensible gas evacuation (10^{-5} Torr) from the heat pipe enclosure before filling. Bubble boiling was not observed in heat pipes with good contact of the capillary wick with the pipe wall. If this contact was poor, however, vapor bubble generation was observed in the regions of poor contact. This phenomenon can be explained by the presence of micro cavities at the pipe wall that were filled by non-condensible gas. The gas molecules were inside cavities in the adsorbed state and were trapped in the cavities by water from the heat pipe volume during the filling process. When contact between the wick and wall was better, fewer cavities were possible as nucleation centers and the highest superheat levels

could be achieved. Another possible reason for boiling in heat pipes with gaps between the envelope and wick is the small amount of nucleation formation time for the gap in comparison to the nucleation formation time for the wick pores $\left(V_{gap} >> V_{pore}\right)$:

$$t_{nc-gap} \sim \left(J_{nc} V_{gap}\right)^{-1} << t_{nc-pore} \sim \left(J_{nc} V_{pore}\right)^{-1} \tag{63}$$

Additionally, liquid in the gap can be stagnant while the liquid in the evaporator wick pores is always replaced during heat pipe operation by returning flow from the condenser.

One of Barthelemy's principle conclusions is that nucleate boiling is not an important mechanism in a well-fabricated heat pipe. Nucleate boiling is justified for heat pipes that operate in temperature regions far from the critical temperature of the working liquid (for instance, water heat pipes in the Barthelemy experiments). As a confirmation of this conclusion, we can also refer to experiments with boiling nucleation in microscale channels conducted by Peng et al. [34]. The liquid superheat temperature in these experiments was the same order of magnitude as that for homogeneous nucleation in an unconstrained liquid. Every pure liquid has a highest attainable temperature for which nucleation will not occur – also called the superheat limit or the explosion temperature (for given pressure conditions). This temperature is closely connected with the concept of liquid tensile strength. As a rule, the superheat temperature for liquid boiling at atmospheric pressure is in the range from $0.8 - 0.95 \times T_c$ [30, p.91]. In this case, the formation of vapor bubbles is connected with the appearance of molecular clusters in liquid. This process is described by kinetic theory.

Today, there are two main approaches to the theoretical calculation of the liquid superheat limit: the "classical" [30, p.75-79] and the model developed by Kwak et al. [35, 36]. The difference is in the conflicting understandings of the surface energy of clusters. In the classical model, the value of liquid surface tension, an equilibrium property of the macroscopic interface, is used. In the Kwak model, surface energy for vapor bubble formation is assigned as the energy required to cut across a cluster composed of activated molecules. Both models can predict the superheat limit with high accuracy. The Kwak model, however, looks more physically realistic and, moreover, allows for the prediction of the decompression level for bubble formation in liquid-gas solutions and of the tensile strength of liquids (which classical theory fails to do). The Kwak model was therefore chosen for superheat limit calculations. The superheat temperature is not dependent on any externally introduced parameters, such as the radius of nucleation site. Instead, the superheat temperature depends only on the physical properties of the liquid and on the operational temperature of the heat pipe (vapor temperature). The superheat temperature does not depend on wick properties directly as in Eq. (61) but does depend on them indirectly. One of the unknown parameters for superheat determination is the nucleation rate J_{nc}. $J_{nc}=10^6$ is considered the threshold of

bubble formation, and $J_{nc}=10^{12}$ nuclei/m^{3}s corresponds to the massive bubble formation according to "classical" superheat limit theory. In practice, however, the nucleation rate for vapor explosion can reach values up to $J_{nc}=10^{28}$ nuclei/m^{3}s [36].

For heat pipes, this threshold nucleation rate can be estimated from the following discourse. If the applied heat rate q is known, we can estimate the time required for liquid replacement in the evaporator zone. Because the nuclear formation time is $\left(J_{nc}\pi r^2(D_1-D_2)/2\right)^{-1}$ (wick is modeled as a series (bundle) of independent parallel cylindrical channels):

$$J_{nc-hp}=\frac{q}{h_{fg}\rho_l\pi\left(r_p\left(D_1-D_2\right)/2\right)^2} \tag{64}$$

After calculation of the superheat limit T_{sh} temperature from the Kwak model and Eq. (63), we can estimate the critical boiling heat transfer:

$$Q_{bmax}^{*}=\frac{2\pi L\lambda_{eff}}{ln\left(D_1/D_2\right)}\left(T_{sh}-T_v\right) \tag{65}$$

The results of modeling (for applied heat rates of q =1 and 10 W/cm^2) are presented in Tables 5 and 6, where n_c is the number of molecules in the critical cluster. If a critical cluster, corresponding to the given conditions, is formed, its growth to a macroscopic vapor bubble is guaranteed.

Table 5. Ammonia boiling parameters (q =1 W/cm^2)

T_v, °C	r_p,micron	$J_{nc\text{-}hp}$, (m^{3}s)$^{-1}$	n_c	T_{sh}-T_v, °C (T_{sh}/T_{cr})	Q_{bmax}^{*},W (q_{bmax}, W/cm^2)
20	1	2.78×10^{11}	2789	74.7 (0.91)	283.4 (3.8)
	2.5	4.45×10^{10}	2902	74.3 (0.91)	281.9 (3.7)
	5	1.11×10^{10}	2990	74.1 (0.91)	281.2 (3.7)
	50	1.11×10^{8}	3281	73.3 (0.90)	278.1 (3.7)
40	1	2.78×10^{11}	2991	57.7 (0.92)	215.4 (2.9)
	2.5	4.45×10^{10}	3113	57.4 (0.92)	214.3 (2.8)
	5	1.11×10^{10}	3206	57.2 (0.92)	213.6 (2.8)
	50	1.11×10^{8}	3520	56.4 (0.91)	210.6 (2.8)
60	1	2.78×10^{11}	3345	42.2 (0.93)	155.1 (2.1)
	2.5	4.45×10^{10}	3482	41.9 (0.93)	154.0 (2.0)
	5	1.11×10^{10}	3587	41.7 (0.93)	153.3 (2.0)
	50	1.11×10^{8}	3941	41.1 (0.92)	151.0 (2.0)

Table 6. Ammonia boiling parameters (q =10 W/cm^2)

T_v, °C	r, micron	$J_{nc\text{-}hp}$, (m^{3}s)$^{-1}$	n_c	T_{sh}-T_v, °C (T_{sh}/T_{cr})	Q_{bmax}, W (q_{bmax} [W/cm^2])
20	1	2.78×10^{12}	2648	75.1 (0.91)	285.0 (3.8)
	2.5	4.45×10^{11}	2760	74.7 (0.91)	283.4 (3.8)
	5	1.11×10^{11}	2846	74.5 (0.91)	282.7 (3.8)
	50	1.11×10^{9}	3134	73.7 (0.90)	279.7 (3.7)
40	1	2.78×10^{12}	2839	58.1 (0.92)	216.9 (2.9)
	2.5	4.45×10^{11}	2960	57.8 (0.92)	215.8 (2.9)
	5	1.11×10^{11}	3052	57.5 (0.92)	214.7 (2.9)
	50	1.11×10^{9}	3363	56.8 (0.91)	212.1 (2.8)
60	1	2.78×10^{12}	3174	42.5 (0.93)	156.2 (2.1)
	2.5	4.45×10^{11}	3310	42.2 (0.93)	155.1 (2.1)
	5	1.11×10^{11}	3413	42.0 (0.93)	154.4 (2.1)
	50	1.11×10^{9}	3762	41.4 (0.92)	152.2 (2.0)

The dependence of the effective pore radius on the critical boiling heat transfer is weak. When the operation temperature of the heat pipe is closer to the critical region, however, it is more important to take the explosive boiling phenomenon into account. In the tables above, it is shown that the heat pipe with an applied heat load of 10 W/cm^2 (Table 6) will not function at the given operational temperatures because it reaches the boiling limitation. The following estimation methods were used for determining the properties of ammonia given a temperature dependence [37]: Carruth-Kobayashi for enthalpy of vaporization, Gunn-Yamada for liquid density, and Lee-Kesler for pressure. The Kwak method for superheat temperature calculation is shown in Appendix 2.

Equation (65) is equitable for ordinary heat pipes when the heat load is applied to the heat pipe enclosure and transferred through the liquid saturated wick to the liquid/vapor phase boundary by conduction. The maximum superheated liquid, in this case, is placed in the region next to the heat pipe enclosure wall. Another situation is realized in LHPs and Capillary Pumped Loops (CPLs). The phase boundary in this case is placed inside the capillary wick, and the distance between the boundary and evaporator enclosure wall is filled by saturated and overheated vapor. It should be mentioned that if LHP/CPL evaporator is designed in such a way that contact between the evaporator wall and the liquid agent is eliminated during LHP/CPL operation then the presence of gas-filled micro cavities at the evaporator wall does not have any influence on boiling initiation in the heat pipe. Thus, if the purity of the working fluid is high, explosive boiling in the evaporator will only start when the superheat limit conditions for the liquid in the capillary wick are reached. From a thermohydraulic analysis of LHP operation [38], the maximum superheated liquid is placed straight under the evaporating inverted meniscus. An analogous thermohydraulic analysis was made by Maidanik et al. [39]. The pressure-

temperature diagram of LHP operation is presented in Fig. 19. According to this diagram, the operational condition of an LHP as a capillary pumped device can be presented in the traditional manner:

$$\Delta P_{cap-max} = \frac{2\sigma}{r_p} \geq \Delta P_{cap} = \Delta P_{LHP} \approx \frac{2\sigma \cos\theta}{r_p} \tag{66}$$

where ΔP_{cap} - capillary head, ΔP_{LHP} - total pressure losses along the circulation loop (including losses in vapor grooves 1-2 [see Fig 19.], vapor line 2-3, liquid line 5-6, and wick 7-8), and θ - meniscus apparent contact angle in the wick. Thus, the explosive boiling condition in an LHP will be:

$$T_v = T_{sh}\left(P_v(T_v) - \Delta P_{cap}\right) \tag{67}$$

and the boiling limit condition will be:

$$\frac{T_v}{T_{sh}\left(P_v(T_v) - \Delta P_{cap}\right)} \leq 1 \tag{68}$$

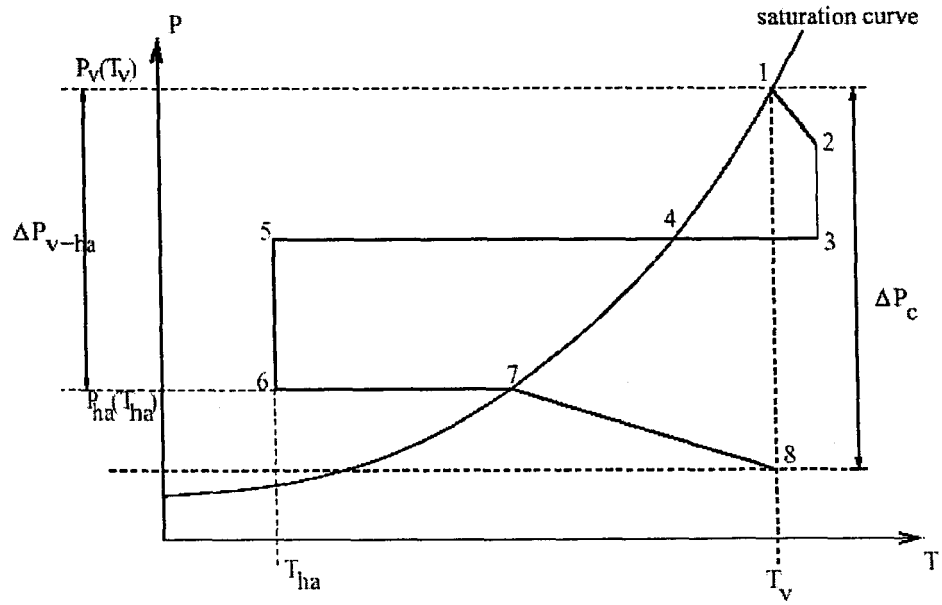

Fig. 19. The pressure-temperature diagram of LHP operation [13].

It is very difficult to reach this limitation because ΔP_{cap}, as a rule, is an order of magnitude or less than 1 bar, and $\left(P_v(T_v) - \Delta P_{cap}\right) \approx P_v(T_v)$ is in the liquid critical region. Consequently, if the LHP/CPL

is fabricated and filled by a working agent with extreme caution and thoroughness, eliminating the presence of non-condensible gases (adsorbed, absorbed, and dissolved) in the system, almost no boiling phenomenon will be realized during LHP operation. It should be mentioned that we are not talking about LHP start-up conditions or regions outside of the wick structure. These problems must be considered separately. Preliminary high static pressurization of the heat pipe envelope (for LHPs – the evaporator) filled by a working liquid can be recommended as one of the stages of the heat pipe manufacturing process.

Mach Number

E. K Levy first theoretically investigated the sonic limitation as a restriction of heat pipe operation in 1968. Since then, every heat pipe theory book has had a paragraph or chapter dedicated to this problem. All researchers emphasize that the sonic limitation is usually important at heat pipe start-up and/or at very low values of the vapor pressure and at high heat loads (high temperature drop between evaporator and condenser). As more heat is applied to the evaporator, the vapor velocity increases accordingly. If the vapor flow becomes sonic, the heat transfer rate becomes constant. This rate does not change with further heat load increases. Thus, the heat flux that results in choked flow corresponds to the sonic limit of heat pipe operation.

The key criterion for the determination of vapor flow type (subsonic or supersonic) is the Mach number. Heat pipes will operate properly if:

$$Ma = \frac{w_v}{v_{sound}} \le 1 \qquad (68)$$

The sound limit critical heat flux for three LHP characteristic elements (channel diameters, see Fig. 2): wick (d), vapor-collecting grooves (d_v), and vapor line (d_h) can be calculated by the equations:

$$Q_{max,d} = \frac{\rho_v h_{fg} D_2 \varepsilon v_{sound}}{(D_2 + 2d_v)}; \qquad Q_{max,d_v} = \frac{\rho_v h_{fg} d_v^{\,2} n v_{sound}}{4L(D_2 + 2d_v)}; \qquad Q_{max,d_h} = \frac{\rho_v h_{fg} d_h^{\,2} v_{sound}}{4L(D_2 + 2d_v)} \qquad (69)$$

where n - number of vapor-collecting grooves and v_{sound} - velocity of sound distribution over saturated vapor at LHP operational temperature.

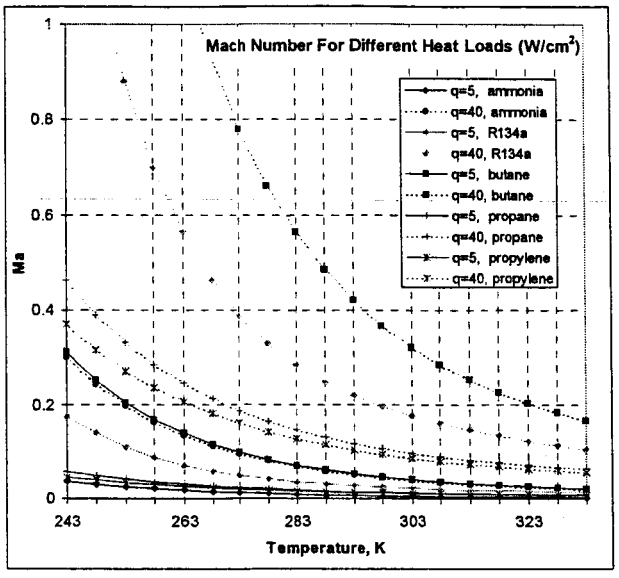

Fig. 20 . Mach Number of different heat loads (5, 40 W/cm^2) and working liquids vs. operational temperature for vapor collecting grooves.

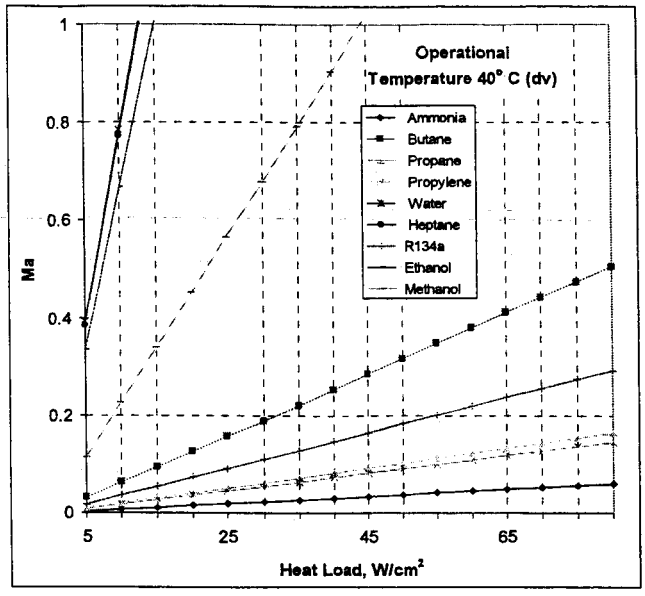

Fig. 21. Mach Number for different heat pipe working fluids as a function of heat load for vapor collecting grooves (operational temperature is 40°C).

For illustrative purposes, the following LHP geometry parameters were chosen: D_2 =24 mm, L_{ev} =100 mm, ε=70%, n=12, d_v=2 mm, d=1 μm. Maximal heat loads, then, for a given configuration and an operational temperature T_v =40°C (ammonia is the working liquid) are: for the wick, 373992 W/cm^2, for the vapor line, 5565 W/cm^2, for the vapor collecting grooves, 2670 W/cm^2. Thus, the vapor collecting grooves are the critical factor from the perspective of sonic limitation. It should be mentioned that in real operation this ammonia LHP could not reach the sonic limit because of other limitations (capillary, for instance). Mach numbers for different heat loads (5, 40 W/cm^2) and working liquids as a function of operational temperature (range –60 - 40°C) for vapor collecting grooves are presented in Fig. 20. As expected, Ma grows as temperature decreases. Obviously (Fig. 20, 21), then, the LHP heat transfer capacity will approach the sonic limit (Ma =1) as the heat load increases.

Finally, we would like to make several remarks about the equation for the calculation of a heat pipe's maximum transport rate density (power per unit of surface) derived by E. K. Levy [8]:

$$Q_{max} = \frac{\rho_v h_{fg} \sqrt{\gamma R_g T_o}}{\sqrt{2(\gamma+1)}} \approx \frac{\rho_v h_{fg} v_{sound}}{\sqrt{2(\gamma+1)}} \qquad (70)$$

Here, we made the reasonable assumption that the temperature in the end of the evaporator T_o for LHP (vapor line beginning) is equal to the LHP operational temperature. The difference between Eqs. (69) and (70), then, is only the presence of a coefficient $\left[2(\gamma+1)\right]^{1/2}$ in (70). If we take into account that for all heat pipe working fluids (cryogenic and low temperature) the heat capacity ratio (γ) is varied between 1 and 4 in the practical and interesting areas of temperatures, we can write condition (49) in the more severe form (the same approach was demonstrated by Peterson [4] for viscous limitation):

$$Ma = \frac{w_v}{v_{sound}} \le 0.1 \tag{71}$$

The heat transfer rates calculated by this formula will always be less than those calculated by Eq. (70) and include some measure of safety. Moreover, in work [4] the other alternative formula for sonic limitation is explained and suggested (this formula was derived by Busse in 1973):

$$Q_{max} = 0.474 h_{fg} \left(\rho_v P_o\right)^{1/2} \tag{72}$$

Because an ideal gas is under discussion we can rewrite Eq. (73) in the following form:

$$Q_{max} = \frac{0.474}{\sqrt{\gamma}} h_{fg} \rho_v \sqrt{\gamma R_g T_o} \tag{73}$$

or:

$$Q_{max} \approx \frac{0.474}{\sqrt{\gamma}} h_{fg} \rho_v v_{sound} \tag{74}$$

This case is also covered by Eq. (71). Thus, using criterion Eq. (71) for engineering purposes appears preferable because of its simplicity and also if the tabulated experimental dependence of the sound speed on temperature is a known function.

Appendix 2. Kwak model for Superheat Temperature Calculation.

First, the J_{nc-hp} from eq. (64) is calculated.

Then, initial data for ammonia are introduced:

P_∞ - Pressure of saturated vapor at operational temperature

ρ_c=225 kg/m^3; T_c=405.35 K –ammonia critical density and temperature,

d_w=2.9×10^{-10} m – Van der Waals diameter of ammonia molecule;

E_i=1.6454E-18 J – Ammonia ionization potential

α=2.6592E-40 J/(V/m)^2 – ammonia polarizability

T_f = 195.42 K- Melting temperature;

ΔH_f =332941.176 J - Enthalpy of fusion;

m = 17 – molar mass;

z=12 – coordination number for FCC lattice

β=1 – accommodation coefficient

$\varepsilon_0 = \dfrac{3E_i\alpha^2}{16d_w^{\,6}}$ - Lennard-Jones potential parameter;

$T_{sh_o} = 0.75 \times T_c$ - Initial value of superheat temperature.

From this point, the iteration cycle for T_{sh} is started.

The following parameters corresponding to T_{sh_o} are calculated:

h_{fg} - Enthalpy of vaporization; ρ_l - density of liquid; $N = {Na\rho_m}/{m}$

$d_m = \left[\dfrac{6 \times 0.7405}{\pi N}\right]^{1/3}$; $V_m = \dfrac{\pi d_m^{\,3}}{6}$ - Average distance between molecules in liquid and effective molecular volume of liquid;

$\varepsilon_m = 4\varepsilon_o\left[1-\left(\dfrac{\rho_c}{\rho_l}\right)^2\right]\left[\left(\dfrac{d_w}{d_m}\right)^6 - \left(\dfrac{d_w}{d_m}\right)^{12}\right]$ - The energy required to separate a pair molecules from d_m to mean distance between molecules at critical point;

$D_e = \beta N\left(\dfrac{8kT_s}{\pi m}\right)^{1/2} exp\left(-\dfrac{h_{fg}}{RT_{sh_o}} - \dfrac{\Delta H_f}{RT_f}\right)\pi\left(\dfrac{3V_m}{4\pi}\right)^{2/3}$ - Coefficient;

$$Z_f = \left[\frac{z\varepsilon_m}{18\pi k T_s}\right]^{1/2}$$ - Zeldovich non-equilibrium factor;

$$n_s = \left(\frac{6kT_s}{z\varepsilon_m} ln\left[\frac{J_{nc-hp}}{ND_e Z_f}\right]\right)^{3/2}$$ - Number of molecules in critical cluster;

$$P_v = \left(\frac{z\varepsilon_m}{3}/V_m\right)/n_s^{1/3} + P_\infty$$ - Vapor pressure;

Now we are determining the temperature T_{sh_1} (which corresponds to obtained P_v)

If $\left|T_{sh_0} - T_{sh_1}\right| > 0.05$ Then $T_{sh_0} = T_{sh_1} + 0.005$, and the cycle is repeated.

Else: final $T_{sh} = T_{sh_x}$. This is the Superheat limit.

ANALYSIS OF TWO-PHASE FLOW IN LHP CONDENSER IN MICROGRAVITY AND EARTH-NORMAL GRAVITY

Two-phase systems for thermal control are currently the most appealing and promising technologies for space applications. Relatively small, autonomous two-phase heat transfer devices such as Heat Pipes (including ordinary grooved or wicked heat pipes, Loop Heat Pipes [LHP], and Capillary Pumped Loops [CPL]) have been successfully adopted for thermal control of different size satellites [40, 41, 42]. In the immediate future, projects of "global," mechanically-pumped two-phase thermal control systems for spacecrafts and segments of the international space station will be realized [43, 44, 45]. Advantages of the two-phase systems over single-phase systems are very well known: an outstanding reduction in mass, size, and energy consumption, and better capability for temperature management as a result of the high isothermal operation of the system. Disadvantages include the complexity of the two-phase systems as well as a lack of theoretical and experimental knowledge, resulting in reduced reliability. Intense efforts by research and scientific institutions are now directed to overcome the above-mentioned imperfections and to develop a new, high-level trustworthy space thermal control scheme.

The condenser is one of the more critical elements of the thermal control two-phase system. Unfortunately, researchers sometimes concentrate on evaporator behavior and underestimate the role of the condenser. Specifically, this neglect is most often apparent in relation to compact and relatively simple two-phase devices, such as the LHP and CPL. The LHP/CPL condenser is usually a part (continuation) of the vapor line or an array of embedded pipes and consists of aluminum or stainless steel cylindrical tubes. It is often suggested that heat transfer is limited by ambient conditions (outside heat transfer coefficient). Pressure drop is also calculated with the help of simplified models of two-phase flow [46] (for quick analyses, engineers even consider this drop as the pressure difference of vapor flow in a pipe with the same length as the condenser) without taking into account the complex nature of the condensation phenomenon and the multipart spectrum of vapor-liquid flow regimes. Moreover, the condenser is usually placed horizontal during earth tests to eliminate gravitational influence. In this case, however, the presence of a stratified flow regime in the condenser is still possible [47]. This regime exists only if gravity force is applied. Thus, we can have gravity-controlled two-phase flow and heat transfer in the condenser even for a horizontal placement.

The first attempt to compare analytically condensation inside tubes under earth gravity and space environments was made by Keshock and Sadeghipour in 1981 [48]. The analogous calculation algorithm is realized in the present work. Keshock and Sadeghipour conducted calculations for refrigerants R12 and R22. In accordance with the chosen methods, a much longer length of tubing (~3 times) is required for

complete condensation under zero-gravity conditions. Keshock and Sadeghipour, however, did not take into account the two-phase flow regime alterations along the condensation length. Only the annular, for the 0-g case, and the stratified, for 1-g regimes, were considered. The chosen models for the heat transfer coefficient and pressure drop determination are not optimal. A large sum of theoretical and experimental information about two-phase flows on earth and (especially) in space conditions has been collected since 1981. This information allows for the modeling of condensation processes with better approaches. Finally, ammonia is currently the primary working thermal agent for space applications. Propylene, butane and R134a can be considered as alternative fluids [49]. Subsequently, the computation and analysis of condensation of the above mentioned liquids for 0- and 1-g conditions hold great practical interest.

By applying an energy balance on an element of the condenser tube, it is possible to write the equation for the distance Δz where condensation of vapor amount $G_{tot}\Delta x$ takes place:

$$\Delta z = \frac{h_{fg} G_{tot} \alpha D}{4 h_z (T_v - T_w)} \Delta x \tag{75}$$

Void fraction variation in the element is neglected. During condensation, the vapor quality x (and void fraction α) varies from 1 to 0. We can divide an unknown condensation length of the pipe by the element Δz (defined by Eq. [75]) with an equal change of the vapor quality Δx. Temperature difference between saturated vapor and wall $(T_v - T_w)$ and total mass flow velocity G_{tot} are given data. To determine the local heat transfer coefficient h_z and the void fraction α, however, information about the two-phase flow regime pattern is required. This information also allows for the calculation of the two-phase flow pressure drop over Δz and the total condensation length. The knowledge of the pressure difference is rather important for the analytical determination of LHP/CPL heat transfer parameters.

Therefore, to investigate analytically the tubeside condensation for micro- and earth-gravity conditions, the appropriate methods for:

- Two-phase flow regime
- Two-phase flow pressure drop
- Local heat transfer coefficient

determination must be chosen and substantiated.

Two-phase flow regime pattern: Earth-Normal gravity case

Detailed two-phase flow regime map analysis related to the condensation phenomenon in horizontal smooth round tubes was made by Dobson and Chato [50]. In this fundamental research, three maps (Mandhane et al. [51], Taitel and Dukler [52], and Soliman [53, 54]) were compared with the experimental results of refrigerants R12, R22, and R134a. All three maps, with certain modifications (for the Mandhane et al. model), some terminology elaboration (for the Taitel-Dukler model), and correct definitions of regimes (for the Soliman model) can be used as good flow regime predictors.

The two-phase flow map for horizontal tube condensation includes eight regimes: annular-mist, annular, wavy-annular, wavy-stratified, smooth-stratified, slug, plug, and bubbly. The overall picture is very complex, but, fortunately, the applied calculations do not require knowledge of all transition lines and criteria among different regimes. Groups of regimes can be described by one model both for pressure drop and for the heat transfer coefficient. Flow character is determined by the relation between gravity and shear stresses (wall-liquid and/or vapor; vapor-liquid interactions) and by the ratio between liquid and vapor velocities.

The Taitel-Dukler model is currently the most theoretically justified and is recommended by the Heat Exchanger Design Handbook [55] as a reliable model for the characterization of adiabatic flow regimes. The relevance of this model to condensing flow demonstrates very good correspondence to the majority of experimental data for freons [51, 56]. Unfortunately, no research has been published dedicated to ammonia tubeside condensation, and only one paper [57] studying adiabatic ammonia two-phase flow patterns was found in the literature. We will consider four areas on the Taitel-Dukler map where both heat and hydraulic performance of two-phase condensing flow can be described by a continued function without jumps: annular (annular-mist and annular regimes), wavy-stratified, smooth-stratified and intermittent-bubble (slug, plug, bubble). The wavy-annular flow can be both in the wavy-stratified region at low, overall mass velocities and in the intermittent region at high velocities. Detailed analysis of the wavy-annular terminology problem can be found in [50].

Chen et al. [57] successfully used the Taitel-Dukler map for the prediction of transitions among annular, wavy-stratified, and intermittent-bubble areas for adiabatic ammonia two-phase flow. The suggested, simplified annular/wavy-stratified transition border as a function of the Lockhart-Martinelli parameter X is used in the presentwork:

$$Fr_{td} = \frac{2.275}{\left(0.7X^2 + 2X + 0.85\right)} \tag{76}$$

where the modified Taitel-Dukler criterion Fr_{td} [58] depends on the Bond number and the vapor Froude number, which is related to the superficial vapor velocity:

$$Fr_{td} = \frac{Fr_v}{\sqrt{1+\frac{1.305}{Bo}}} \tag{77}$$

This criterion is different from the one originally suggested by Taitel and Dukler and takes surface tension forces into account. Surface tension is very important for flow in small diameter tubes (>3 mm). The original Taitel-Dukler map is used to predict intermittent to annular transition for small tubes cases [59].

The border between annular and intermittent-bubbly areas is X=1.25. This is the average value suggested by Breber et al. [56] with a transitional area limited by the lines X=1 and X=1.5. The regions of wavy-stratified and smooth-stratified flows are divided by criterion [52]:

$$K_{td} = Fr_{td}\sqrt{Re_l} \geq \frac{20}{j_v\sqrt{j_l}} \tag{78}$$

Finally, it should be mentioned, although widely found in textbooks, the flow pattern map of Baker [60] has a historical value as a first map but is a poor predictor for regimes of condensing [61] and adiabatic [65] two-phase flows.

Two-phase flow regime pattern: Microgravity case

The absence of gravity leads to a simplification of the overall two-phase flow map. Only three main regimes were observed by researchers: bubble, slug, and annular. More detailed flow classification, however, can be find in the literature [62]: dispersed bubble, bubble, slug, slug-annular transitional, and annular. To complete the picture, we can divide annular flow into three regions: smooth-annular, wavy-annular, and mist. Reinarts et. al. [63] classified smooth- and wavy-annular regimes as "small tube" and "large tube" flow behavior. Research on condensing flow regimes for water was intensively conducted in Texas A&M University [64]. In the research, there existed one work on ammonia condensing flow investigation, which was carried out under the guidance of the European Space Agency [45]. Unfortunately, the description of ammonia condensation flow patterns and condensation length comprised only one paragraph in the paper, leaving it rather difficult to make any conclusions based on the given information. Many adiabatic flow experiments have been made in microgravity conditions in the last two decades. The most popular medium was an air-water mixture [65, 66, 67, 68]. Different additives to water

were used to vary liquid viscosity and surface tension [69,70]. The experiments with single-component, adiabatic, two-phase flow in microgravity were conducted for freons R12 [71], R114 [72], and ammonia [63]. The ratio of vapor and liquid densities has an influence on the flow behavior, subsequently giving the data for single components priority meaning for our investigation. As mentioned by Reinarts and Ungar [73], the experimental database for R12 is the most extensive and gives a substantive definition of slug to annular transition.

For the purposes of the present work, only two transition criteria are important: slug-annular/smooth-annular and smooth-annular/wavy-annular. Because a pressure drop in this area can be distinguished several times, different analytical models are required. Moreover, bubble, slug, and slug-annular regimes (the last pattern includes in itself a frothy slug-annular regime reported by Zhao and Rezkallah [65]) usually took relatively small parts of the total condensation length and can all be well described by homogeneous pressure drop models.

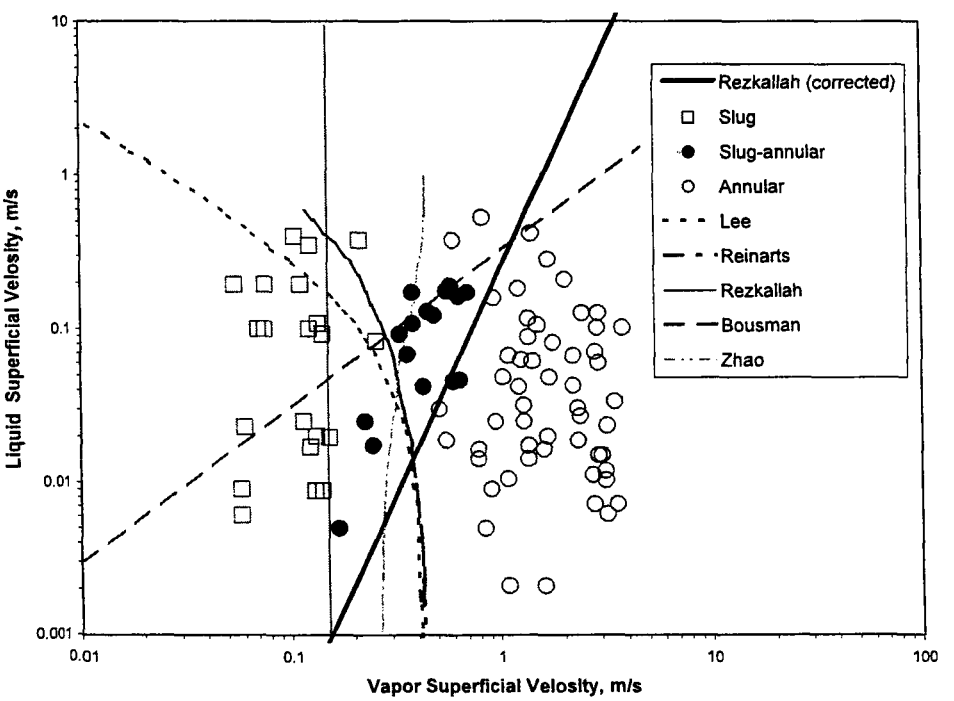

Fig.22 Slug-annular microgravity transition models and R12 databank (ID=10.5 mm)

After the analysis of several microgravity two-phase flow-pattern maps the Weber number based map of Rezkallah [74] was chosen as the most experimentally justified map. Rezkallah demonstrated, what practically all knew (before 1996), that air-water mixture flow data have a border between transition slug-annular and annular regimes at $We_g \sim 20$. Gas Weber numbers, however, must be calculated for actual gas velocity. Superficial velocities of gas (vapor) and liquid are known from experiments as a rule.

To determine the actual velocities, knowledge of the void fraction value is needed. This is a difficult problem for both analytical and experimental consideration (see, for instance, [75]). The transition line has a positive slope if coordinates of the two-phase flow-pattern map are gas and liquid Weber numbers based on superficial velocities. Taking into account experimental data from [76], the criterion for slug-annular and annular regimes change can be written as:

$$We_{gs} \leq 7.94 We_{ls}^{0.34} \tag{79}$$

Thus, two empirical constants are presented in the model. Practically, all microgravity two-phase flow patterns maps available in the literature have only a semi-theoretical character. In microgravity, the ratios among three forces: inertia, viscosity, and surface tension are important. Three dimensionless groups can be used for analysis of two-phase flow regimes: Weber, Suratman, and Reynolds [77]. Because every number is defined in relation to the other two, only two numbers are needed for the modeling of regimes transitions. Rezkallah [74] claims that the relation between inertia and surface tension holds primary meaning, while Jayawardena et al. [78] used a combination of Re and Su numbers for the gas and liquid phases and two empirical constants for microgravity map development. The Jayawardena et al. model is more complex but has no real advantages over the Rezkallah model. Several slug-annular transition models based on force balances were suggested including Bousman void fraction matching criteria [68] and the Lee model of surface tension/inertia balance [79], which was later improved by Reinarts [71]. More recently, one more model on the slug to annular transition (based on the drift-flux relation between superficial velocities and void fractions) was suggested [80]. All models need the following constants that must be determined from experiments: the vapor-liquid interface friction factor f_i and/or the critical void fraction α_{cr}, and/or the distribution coefficient C_o, and the dimensionless factor k. The physical origin of all mentioned models (except perhaps for the Jayawardena et al. model) is the same. An experiment, therefore, is the only criterion. Experimental data for one component two-phase flow R12 and different modeling transition lines are shown in Fig. 22. It is clear that the Rezkallah (corrected) line divides annular and slug-annular areas better then any another transition border. A common misunderstanding [66, 73] in this case is the use of superficial instead of actual velocities for Weber number calculation in the Rezkallah model (Rezkallah on Fig. 22). It should be mentioned that data for R114 also agree well with eq. (79) (Fig. 23).

Two-phase microgravity experiments with ammonia were conducted for the small diameter tube (3.34 mm) [63]. It was found that 0-g and 1-g pressure drops for given conditions do not have any systematic differences. In addition, the authors reported on the presence of two regimes ("large tube" and

"small tube") where pressure drops were well described by smooth-annular and wavy-annular models. The transition lies somewhere in the area $10<We_{gs}<100$. Unfortunately, there is currently not enough experimental material to determine this border with a good approach. Based on this experiment and the Rezkallah *We* number model, however, we defined the smooth to wavy annular transition criteria as:

$$We_{gs} \le 16 We_{ls}^{0.34} \tag{80}$$

The borders between different regimes are shown in Fig. 23.

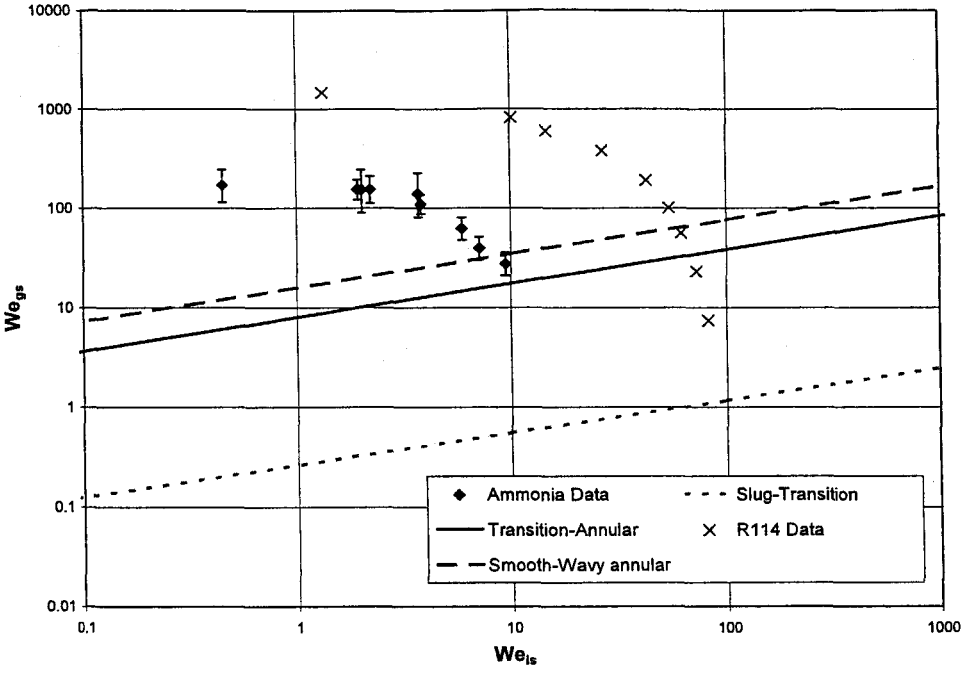

Fig.23 Rezkallah model and smooth-wavy annular transition lines, ammonia (ID=3.34 mm) and R114 (ID=15.4 mm) data.

Two-phase flow Pressure drop: Earth-Normal gravity case

The two-phase pressure drop depends on the flow regime. The following pressure drop models were chosen as the most experimentally verified models:

- Annular (all) regimes: Tronievski and Ulbrich [81]
- Wavy-stratified: Taitel and Dukler [82] with ratio $f_l/f_v=1$ [83].
- Smooth-stratified: Taitel and Dukler [82] with ratio $f_l/f_v=10$ [84].
- Slug, plug, and bubbly: Beattie and Whalley [85].

Short mathematical presentations of all of the above mentioned models can be found in [86]. The Tronievski and Ulbrich model is a series of exponential and polynomial empirical formulas for different ranges of the Lockhart-Martinelli parameter but with minimal error [87]. This model has also demonstrated very good agreement with recent ammonia [57] and R114 [86] annular flow regime experimental observations. The Taitel and Dukler model is based on momentum balance equations for equilibrium stratified two-phase flow, but the experimental vapor-liquid interfacial friction ratio f_i/f_v is required. Chosen values (1 for smooth stratified and 10 for wavy stratified regime) were based on large amounts of experimental data. The number of homogeneous models in which two-phase flow was considered a uniform medium is available in the literature [88]. Most commonly, models have the least error when the vapor velocity is not significantly different from the liquid velocity. This general rule of thumb is valid for slug, plug, and bubbly regimes. The most common homogeneous approach is the McAdams model [55]. The Beattie and Whalley model was selected, however, because of this technique, which was originally developed as a model for a wide range of flow regimes including intermittent and transient to annular. Relatively new experimental data for R113 [89]are also evidence of the ability of the Beattie and Whalley model to adjust well to cases of low mass fluxes and low vapor qualities.

Two-phase flow Pressure drop: Microgravity case

The Method presented by Chen et al. [86] with an empirical equation for interfacial friction ratio [84]:

$$\frac{f_i}{f_v} = 1 + 6.81(1-\alpha)^{0.39} \tag{82}$$

was used for wavy-annular flow prediction of the pressure drop. This model correlated well to almost all known experimental data. For the smooth-annular regime region, the same method was applied, but the interfacial friction ratio was equal to unity [63]. It should be mentioned that Tronievski and Ulbrich and Chen et al. methods usually give very close results for two-phase annular patterns (for both Earth-normal and microgravity cases). These results are logical because the presence of annular flow in Earth environments means that gravity force is negligible and cannot stratify the flow. Different approaches for the annular regime are used because the Tronievski and Ulbrich model is originally based on the large, normal-gravity experimental databank while the Chen et al. model is related to experimental records for microgravity. According to these data [86], the pressure gradient is higher in microgravity conditions. This conclusion (and the quality of the experiment setting in [86]) is criticized by Shungar et al. [90].On the basis of Earth experiments with water-benzoate annular flow, which (as the authors supposed) are

simulating the behavior of R11 in microgravity, Shungar et al. claim that the two-phase pressure drop in a 0-g environment must be 2-3 times less than it is in 1-g conditions. First, from the point of view of the authors, the claims of Shungar et al. are true if the discussion centers on smooth-annular flow. Ordinarily, however, the wavy-annular regime is presented in microgravity conditions. The majority of the Chen et al. experimental points belong to this area (see Fig.23). Second, the average annular flow film thickness is greater in microgravity conditions (uniform film). Thus, waves can have higher amplitude, and average interfacial shear stress will be greater. Principally, there are no reasons to doubt the experimental data for R114 from [86].

As for normal gravity, the homogeneous Beattie and Whalley model for pressure drop prediction was used in bubble, slug and transitional flow regimes in microgravity. The correctness of such an approach is confirmed in [91].

All presented above methods for pressure gradient calculation are frictional models which are equitable for adiabatic flows without mass flow between phases due to condensation. In practice, condensation leads to a reduction of interfacial shear stress and thus to a reduction in pressure drop. To take this phenomenon into account, the method of interfacial shear stress correction [92 p.338] based on the "Reynolds flux" concept [93 p. 164] was realized.

Local Heat Transfer Coefficient: Earth -Normal Gravity Case

It is common practice to divide the phenomenon of condensation inside tubes into two regions: gravity-controlled and shear-stress-controlled (or annular flow) condensation [50]. For both areas a number of different correlations for the local heat transfer coefficient is available. Because we could not find any experimental data for ammonia (a recent fundamental review of available correlations for two-phase flow heat transfer of ammonia made by Ohadi et al. [94] mentioned only one empirical formula [95] related to condensation inside finned air-cooled tubes) we must select a model most appropriate for our case from known generalized correlations obtained from experiments with other fluids. Below, we consider a series of models for horizontal two-phase condensing annular flow.

One of the older and more widely used models is the correlation based on experiments with R11, R12, R21, R22, R113, and R114 suggested by Cavillini and Zecchin [96]:

$$Nu_z = 0.05 Re_{eq}^{0.8} Pr_l^{0.33} \tag{83}$$

where the equivalent Reynolds number Re_{eq} is:

$$Re_{eq} = Re_v \left(\mu_v/\mu_l\right)\left(\rho_l/\rho_v\right)^{0.5} + Re_l \tag{84}$$

Vrable et al. [97] tried to take into account the pressure influence on the heat transfer coefficient and modified Eq. (83) based on their own R12 experiments:

$$Nu_z = 0.015 P_{re}^{-0.65} Re_{eq}^{0.8} Pr_l^{0.33} \tag{85}$$

Later, Shah [98], after analysis of a large databank that includes experimental points for refrigerants, water, methanol, benzene, toluene trichlorethylene, and ethanol, obtained the following correlation:

$$Nu_z = 0.023 Re_l^{0.8} Pr_l^{0.4} \left(1 + \frac{3.8}{P_{re}^{0.38}} \left(\frac{x}{1-x}\right)^{0.76}\right) \tag{86}$$

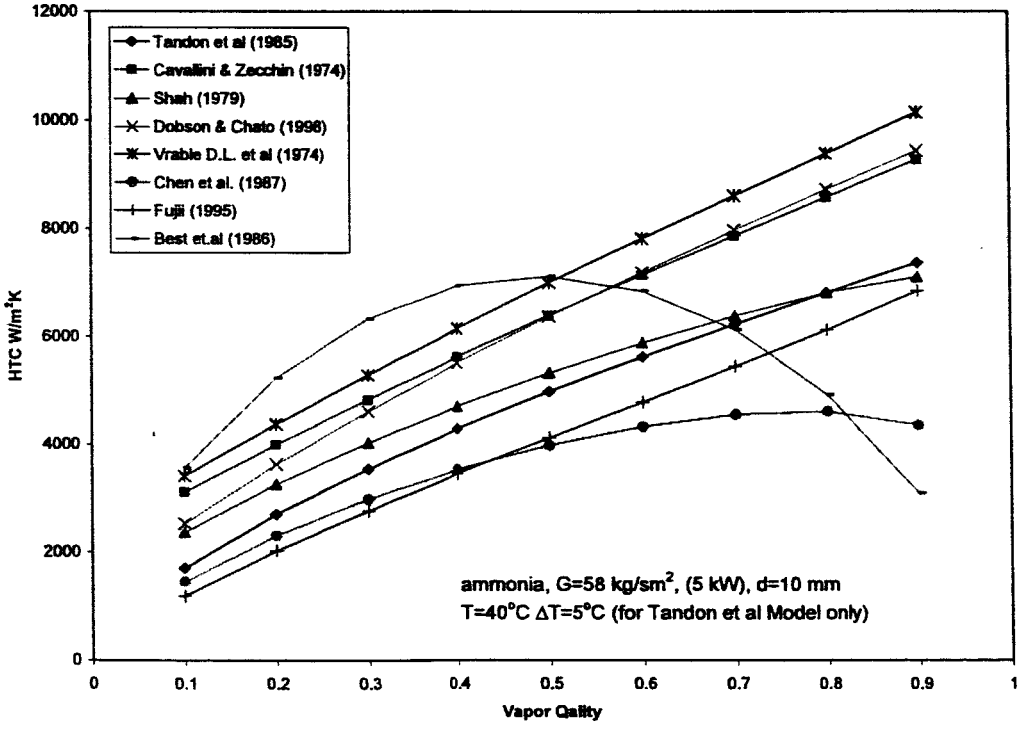

Fig.24 Annular condensing flow heat transfer coefficient vs vapor quality prediction by different models for ammonia.

Dobson and Chato [50] recommended a model which depends on the turbulent-turbulent Lockhart-Martinelli parameter (experiments with refrigerants R12, R22, R-134a, and near-azeotropic blends of R32/R125):

$$Nu_z = 0.023 Re_l^{0.8} Pr_l^{0.4} \left(1 + \frac{2.22}{X_{tt}^{0.89}}\right) \tag{87}$$

Based on experimental results for R22, R134a, and R123, Fujii [99] suggested another Nusselt number expression:

$$Nu_z = 0.0125 \left(Re_l \sqrt{\rho_l/\rho_v}\right)^{0.9} \left(x/1-x\right)^{0.1x+0.8} Pr_l^{0.63} \tag{88}$$

Chen et al. [100] developed a model for vertical shear stress controlled flow, which, because of its generalized character, must be valid for the horizontal annular flow regime:

$$Nu_z = 0.018 \left(\rho_l/\rho_v\right)^{0.39} \left(\mu_v/\mu_l\right)^{0.078} Re_l^{0.2} \left[Re_{lo} - Re_l\right]^{0.7} Pr_l^{0.65} \tag{89}$$

Finally, despite the fact that Shah concluded in his critical review [101] that the model [102] is clearly unsatisfactory, the Ackers and Rosson model is still recommended by ASHRAE [103, p.4.8] as the primary model. Originally, the Ackers and Rossin correlation was based on R12, methanol, and propane data. In the present paper, we used a modified Tandon et al. [104] formula (experiments with R12 and R22). The difference between the Tandon et al. equation from the Ackers and Rossin equation is only the difference inconstants, 0.084 instead of 0.1:

$$Nu_z = 0.084 Pr_l^{0.33} Ja^{0.17} Re^{\bullet}_v{}^{0.67} \quad , \quad Re^{\bullet}_v = \frac{DG_v}{\mu_l}\sqrt{\frac{\rho_l}{\rho_v}} \tag{90}$$

The local heat transfer coefficient depends on the latent heat of vaporization (Jacobs number) only in this model. Taking into account that the latent heat for ammonia is much greater than it is for any freon, the dependence of the local heat transfer coefficient on the latent heat of vaporization can be important.

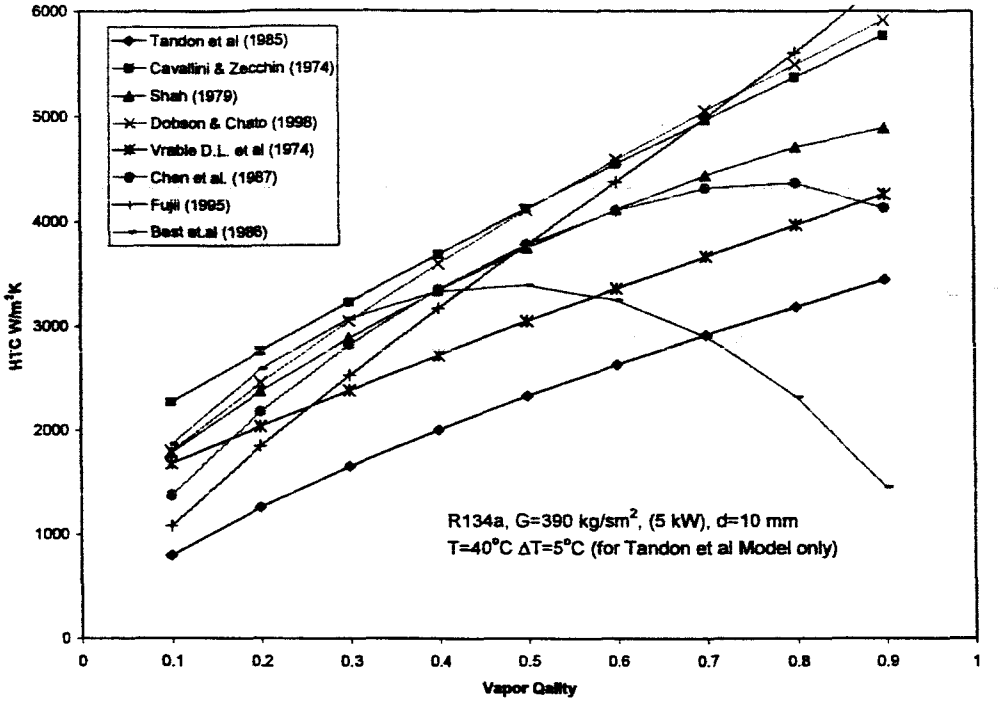

Fig.25 Annular condensing flow heat transfer coefficient vs vapor quality prediction by different models for R134a.

After a comparison of the different models, the Shah correlation was chosen for ammonia annular condensation heat transfer prediction as an average model (see Fig.24 and Fig. 25). The result is expected because eq. (86) is based on the largest experimental databank.

The region of gravity-controlled condensation was divided into two regions corresponding to wavy flow and smooth two-phase flow regimes. Four models are related to wavy flow correlations: Dobson [105], Rosson and Meyers [106], Ackers and Rosson [102], and Tandon et al [104]. Actually, all of the models listed above are recommended for all gravity-controlled condensation regions, but correlations have the smallest error in the wavy region when liquid and/or vapor flows are turbulent (in the models of Dobson and Rosson–Meyers, the turbulent-turbulent and the laminar-turbulent Lockhart-Martinelli parameters were used). Ackers-Rosson and Tandon et al. approaches have a poor physical background and are based on data from refrigerants R12 and R22. The Rosson-Meyers method has the disadvantage of being complex and reliant upon empirical (based on a limited amount of data) equations for the calculation of the fraction of circumference where filmwise condensations prevail. The Dobson model was grounded on an idea analogous to the idea on which the Rosson-Meyers model was grounded but is less complex and more experimentally proofed. The Dobson correlation was selected for our investigation:

$$Nu_z = \frac{0.23 Re_{vo}^{0.12}}{1+1.11 X_{tt}^{0.58}} \left[\frac{Ga Pr_l}{Ja_l} \right] + \left(1 - \frac{\theta_l}{\pi} \right) Nu_{forced} \tag{91}$$

$$Nu_{forced} = 0.0195 Re_l^{0.8} Pr_l^{0.4} \sqrt{1.376 + c_1 X_{tt}^{-c_2}} \tag{92}$$

For $0<Fr_l<0.7$,

$$c_1 = 4.172 + 5.48 Fr_l - 1.564 Fr_l^2, \quad c_2 = 1.773 - 0.169 Fr_l \tag{93}$$

For $Fr_l>0.7$,

$$c_1 = 7.242, \quad c_2 = 1.655 \tag{94}$$

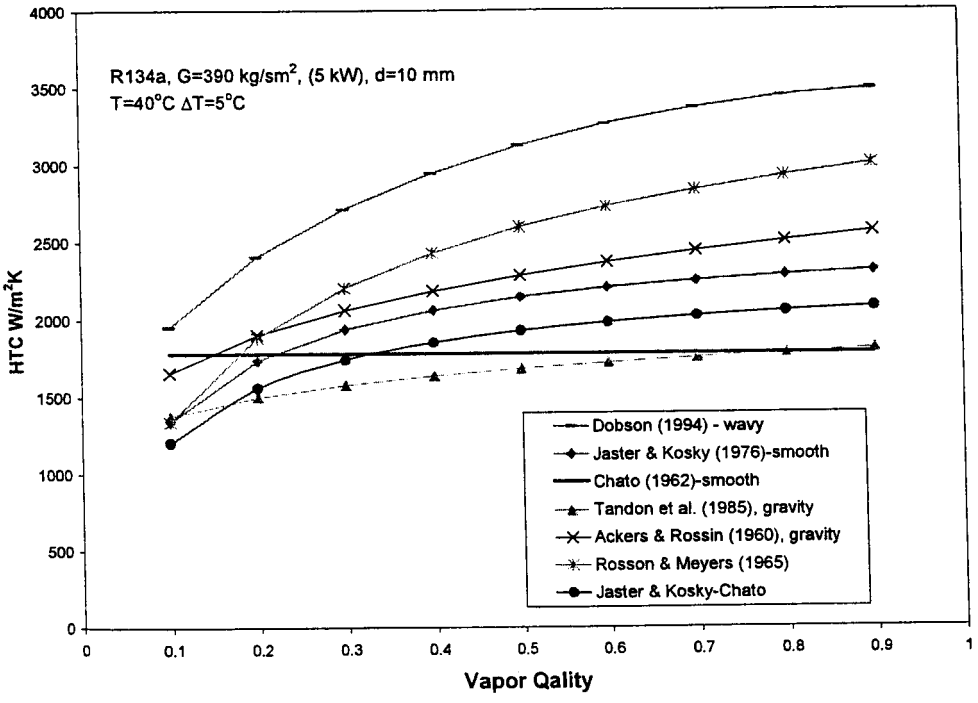

Fig.26 Gravity-controlled condensing flow heat transfer coefficient vs vapor quality prediction by different models for R134a.

The angle subtended from the top of the tube to the liquid level θ_l is calculated from the equation for the void fraction, which is known from the pressure drop model calculation:

$$\alpha = \frac{\theta_l}{\pi} - \frac{sin(2\theta_l)}{2\pi} \tag{95}$$

For condensation in conditions with smooth stratified and intermittent flows, a combined correlation of Chato [107] and Jaster and Kosky [108] was used. Both models are modified Nusselt formulas for gravity-driven condensation on a vertical plate. The Chato model usually correlates well with experimental data but does not have a dependence on the void fraction (vapor quality) in its simplified form:

$$Nu_z = 0.555\left[\frac{\rho_l(\rho_l-\rho_v)gh_{fg}'(1+Ja_l)D^3}{\lambda_l\mu_l(T_v-T_w)}\right] \tag{96}$$

where $h_{fg}'=h_{fg}(1+0.68Ja_l)$ is the Rohsenow modified latent heat [50].

The formula suggested by Jaster and Kosky, as a rule, overpredicts the heat transfer coefficient [101]:

$$Nu_z = 0.728\alpha^{3/4}\left[\frac{\rho_l(\rho_l-\rho_v)gh_{fg}'(1+Ja_l)D^3}{\lambda_l\mu_l(T_v-T_w)}\right] \tag{97}$$

Taking into account the fact that the simplified Chato equation was obtained for an average angle of θ_l=120° and the dependence between the void fraction and this angle (95), we can correct the constant in Eq. (97) by multiplying it by 0.9. Dependences of the heat transfer coefficients from the above -discussed models for gravity-controlled condensation on vapor quality are presented in Fig. 26.

Local Heat Transfer Coefficient: Microgravity Case

The Shah correlation for two-phase annular flow heat transfer coefficients was extrapolated to the microgravity case. From physical consideration, there are no principal differences between annular approaches for Earth-normal gravity and microgravity cases. Moreover, the validity of the chosen approach is confirmed by experiments conducted by Kachnik et al. with R12 in microgravity conditions [64]. In the area of low vapor qualities, the experimental points were well predicted by the Eq. [109]:

$$Nu_z = 0.023Re_l^{0.8}Pr^{0.3}\left(1+x\frac{\rho_l}{\rho_v}\right)^{0.8} \tag{98}$$

In Fig. 25 (R134a), the Best correlation in the region of low vapor quality practically coincides with the line calculated by the Shah model. Equation (98), however, is hardly valid for ammonia condensation (Fig. 24).

The summary of selected methods for two-phase, condensing flow modeling in Earth-normal gravity and microgravity conditions is presented in Table 7.

Table 7. Selected methods for two-phase flow, condensing flow modeling

	Tubeside Condensation						
	1-g (horizontal) case			0-g case			
	Flow Regimes	Pressure Drop	Heat Transfer	Heat Transfer	Pressure Drop	Flow Regimes	
Taitel-Dukler Map [52]	Annular	Tronievski-Ulbrich [81]	Shah [98]	Shah[98]	Chen et al. [86] f_l/f_V=f(α) Eq.(82)	Wavy-Annular	Rezkallah Map [74]
	Wavy-Stratified	Taitel-Dukler [82] f_l/f_V=10	Dobson [105]		Chen etal. [86] f_l/f_V=1	Smooth-Annular	
	Smooth-Stratified	Taitel-Dukler [82] f_l/f_V=1	Chato & Jaster-Kosky		Beattie-Whalley [85]	Bubble, Intermittent	
	Bubble, Intermittent	Beattie-Whalley [85]					

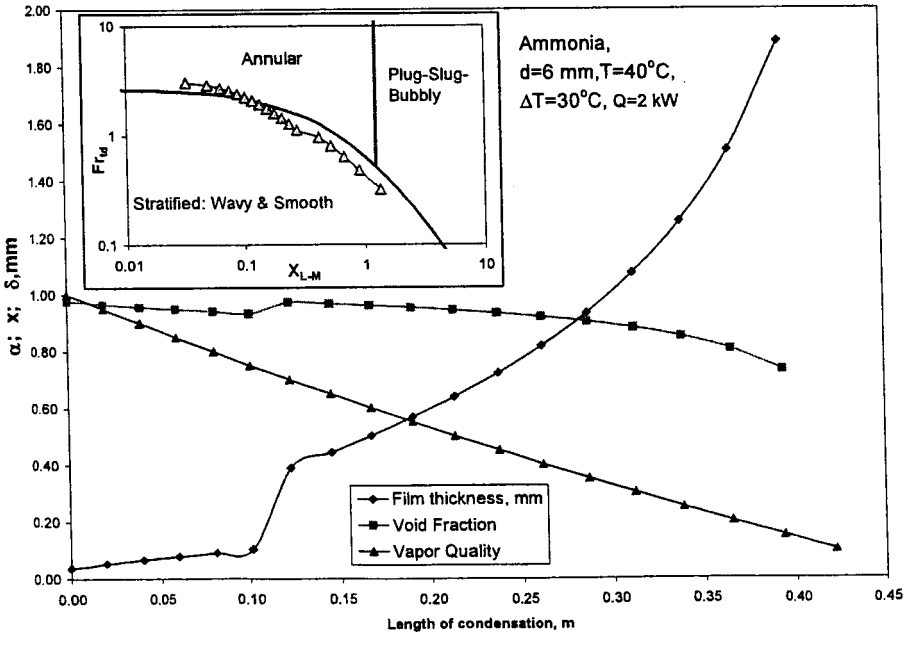

Fig.27 Condensate film thickness, void fraction, and vapor quality vs length of condensation for gravity–controlled, condensing two-phase flow.

Results and discussion

Applying the techniques selected herein, the following types of result have been calculated:

- Length of tube to achieve complete condensation;
- Overall pressure drop on length of condensation;
- Film thickness, void fraction, and vapor quality change during condensation.

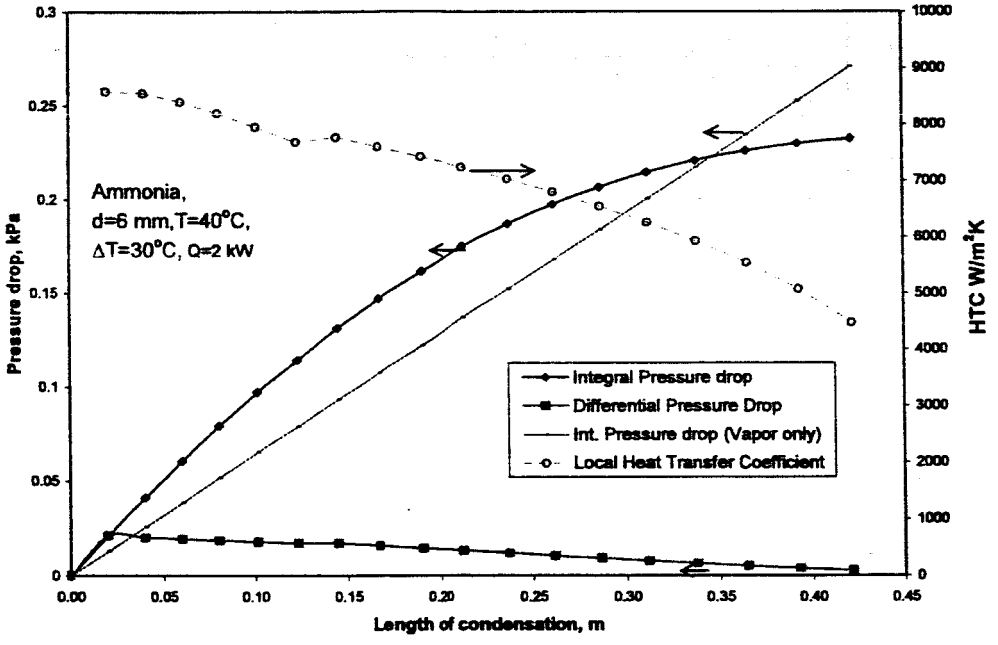

Fig.28 Integral and differential pressure drops and local heat transfer coefficient vs length of condensation for condensing two-phase flow in Earth-normal gravity conditions.

The following parameters were selected as a basis for our investigation: working liquid – ammonia, vapor temperature – 40°C, wall temperature of the condenser – 10°C, LHP heat load – 2000 W, inner diameter of the condenser tube – 6 mm. Results of calculations for the Earth-normal gravity case are shown in Fig. 27 and in Fig. 28. Two flow regimes, annular and wavy-stratified, are realized for the given conditions (see Fig. 27, Taitel-Dukler map with condensation path). The transition vapor quality value is about 0.7 (the distance from the condenser inlet is ~120 mm). After this border, instead of the annular film thickness, the depth of the stratified liquid layer is presented on the graph. The local heat transfer coefficient and integral and differential pressure gradients along the condenser tube also depend on the flow regime character (Fig.28). For illustrative purposes, the pressure drop of only vapor flow along the tube is shown. During the process of condensation, the two-phase pressure drop can be considerably higher than the "vapor-only" line, but the final overall pressure drop on total condensation length (0.42 m) is less and is not far from the value of the vapor flow pressure difference. The pressure drops, the heat transfer coefficient for microgravity conditions along the length of condensation, and the condensation

path on the Rezkallah map are demonstrated in Fig. 29. Overall condensation length is only about 10% more than it is for the 1-g case. Pressure drops in 0-g and 1-g conditions are also not much different. Thus, the behavior of the condenser in space for the selected set of input parameters will be almost the same as it is in its Earth-horizontal position.

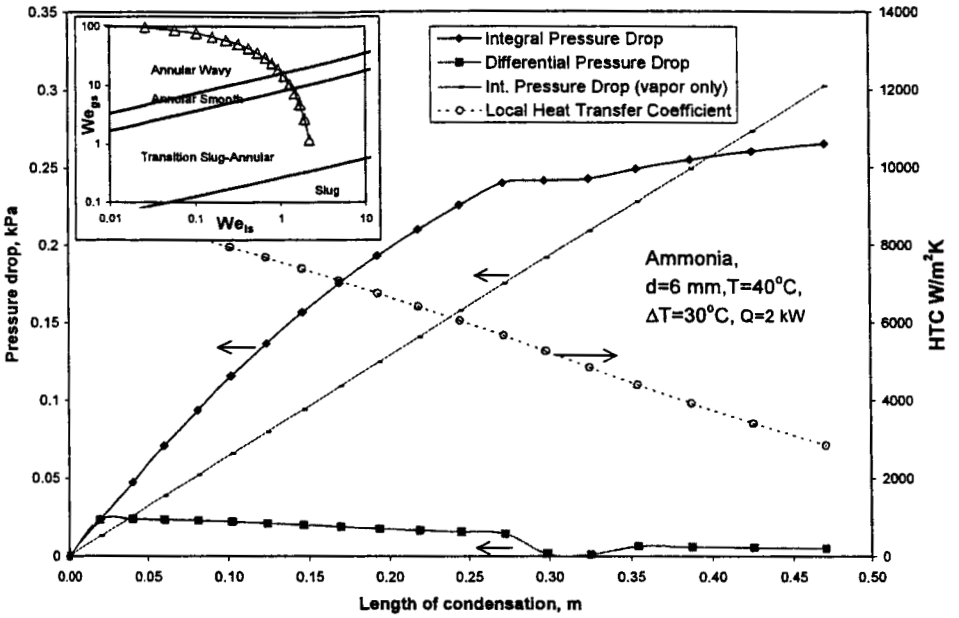

Fig.29 Integral and differential pressure drops and local heat transfer coefficient vs length of condensation for condensing two-phase flow in microgravity conditions.

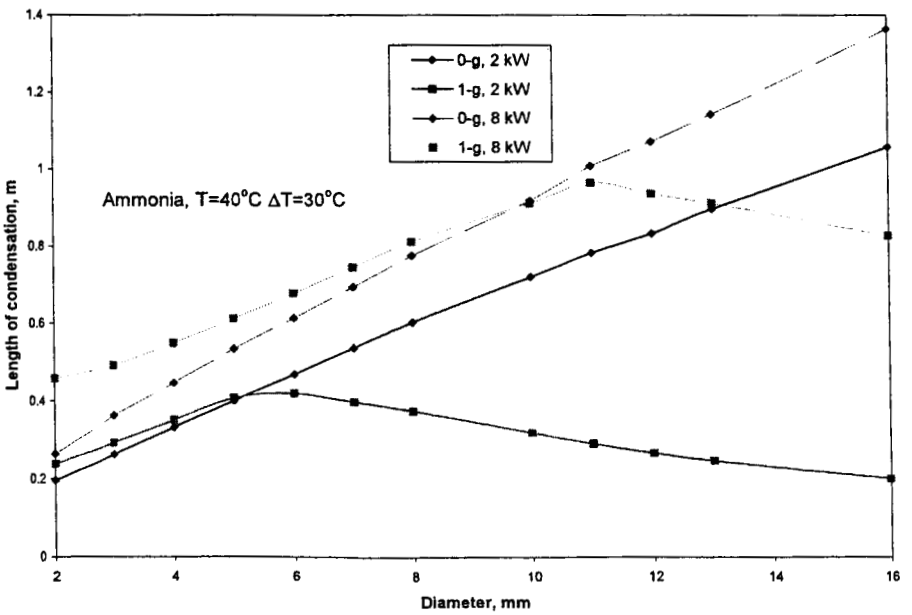

Fig.30 Condensation length for different condenser tube diameters and heat loads in microgravity and Earth-normal gravity conditions.

The considered case, however, is a "unique" situation. The condensation length can be less than or considerably more than it is in space conditions. This effect is illustrated in Fig. 30. For a 16 mm diameter pipe, the condensation length in microgravity is 1.7 (8 kW) – 5 (five!) (2 kW) times higher than it is in an Earth environment. In ammonia pressure drops for micro- and normal gravities, the differences are not so large, particularly because of the areas of small diameters and/or high heat fluxes (Fig. 31). The variation between pressure gradients calculated by the adiabatic flow model and by the model that takes into account the influence of mass flow caused by condensation is in the range from 3-20%. The condensation phenomenon leads to a pressure drop reduction. It is remarkable that acceptable values result, for given conditions of the rough approach, when the two-phase flow pressure drop in the condenser is replaced by the vapor flow pressure drop of the same distance. Results are not valid, however, if the working liquid is not ammonia but is, for instance, propylene (Fig 32). From Fig. 32, it is clear that R134a has the biggest pressure gradient and that ammonia has the smallest pressure gradient if other conditions are the same. This relationship is natural in that ammonia has the largest latent heat of evaporation, which leads to a smaller total mass flux, when compared with propylene and R134a.

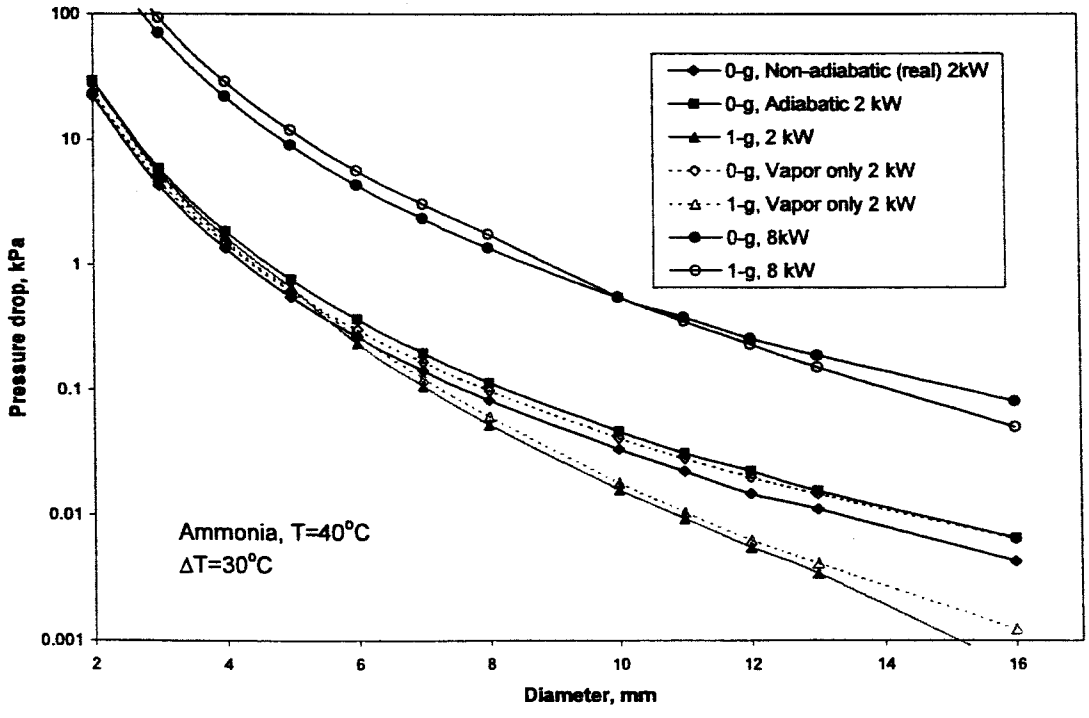

Fig.31 Overall pressure drops on condensation lengths for different condenser tube diameters and heat loads in microgravity and Earth-normal gravity conditions.

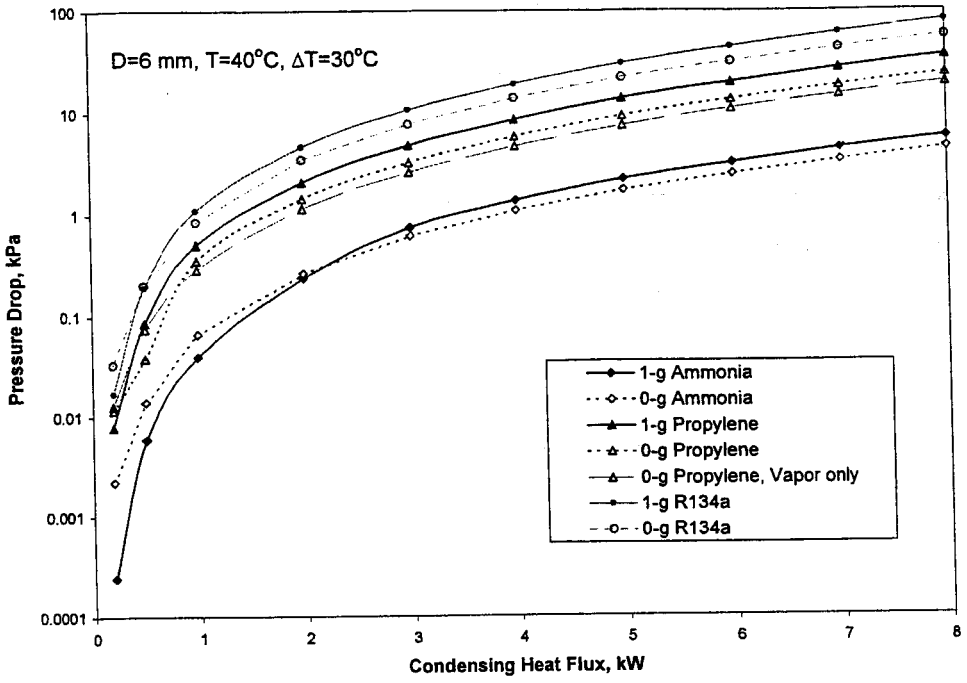

Fig.32 Overall pressure drops on condensation lengths vs. heat loads for ammonia, propylene, and R134a in microgravity and Earth-normal gravity conditions.

CONCLUSIONS

Application of dimensionless analysis techniques in the field of LHP theory and practice allows for the examination of scaling issues in LHP with a special focus on individual components (liquid and vapor lines and evaporators).

The Buckingham π-Theorem is useful for deriving non-dimensional groups and (especially) geometrical ratios as shown by an example of the liquid-line scaling. One and two-dimensional LHP evaporator models based on energy equations take convection effects into account and are applied to derive non-dimensional groups that can be used for scaling. Examples for such scaling are presented, both for fluid to fluid and for geometrical scaling.

A set of dimensionless criteria for LHP design and operation were noted and analyzed in the second part of the work. Criteria were based on general dimensionless numbers from heat and mass transfer theory, heat pipe operational limitations adopted for LHP conditions, and LHP specific features. The use of dimensionless analysis provides a better understanding of the physical phenomena in LHP and better means for the comparison and generalization of data.

The presented set of dimensionless criteria can be used as an effective instrument of LHP scaling design and operation analysis, which allows for the defining of the main physical processes in LHP, for the estimation of the values and magnitudes of different forces, for the selection of a working fluid (group of fluids), and for the development of an LHP evaporator prototype drawing. This set can be a useful analytic tool for the advance of complex mathematical modeling using thermal-fluid differential equations.

Furthermore, utilizing these dimensionless groups, scaling issues for reduction of size can be determined and evaluated, thus aiding the development of miniature LHPs.

Finally, a detailed analysis of recent models and experimental data for condensing two-phase flow regimes, pressure gradients, and local heat transfer coefficients in Earth-normal gravity and microgravity conditions was made, and the results were summarized in Table 7. Based on the selected methods, the analytical investigation of ammonia, propylene, and R134a two-phase condensing flow performances was carried out. Special attention was given to pressure gradients and condensation lengths.

It was found that:

- The length of condensation in microgravity at certain conditions can be larger than the length of condensation for a 1-g horizontal tube by several (even ten) times. The situation when lengths are equal can also be realized (see Fig. 30).

- Pressure drops in the condenser for micro- and normal gravity surroundings are not significantly different, particularly because of their relationship to areas of small diameters and/or high heat fluxes
- The engineering rough approach, when the two-phase flow pressure drop in the condenser is replaced by the vapor flow pressure drop over the same distance, can give acceptable results for ammonia condenser design calculations but is not valid in general for other working fluids and is different from those considered in the paper operational conditions.

The verification of obtained results by experimental efforts, especially for ammonia local heat transfer coefficients for condensation in tubes and annuli for both 1-g and micro-g environments, is extremely desired. The derived scaling relations in the first part of the report must also be verified in experimental studies as well.

REFERENCES

1. Delil, A.A.M. "Thermal-Gravitational Modeling and Scaling of Heat Transport Systems for Applications in Different Gravity Environments: Super-Gravity Levels & Oscillating Heat Transfer Devices," SAE Paper 2000-01-2377, 2000.
2. Kiseev, V. and Pogorelov, N. "A Study of Loop Heat Pipe Thermal Resistance," 10th International Heat Pipe Conference, Stuttgart, Germany, September 1997.
3. Fershtater,Y. and Maidanik, Y. "Analysis of the Temperature field in the capillary Strucure of an Antigravitational Heat Pipe," J. Eng. Phys., Vol. 51, pp. 897-900, 1986
4. Peterson, G. P., *An Introduction to Heat Pipes: Modeling, Testing, and Applications,* John Wiley & Sons, New York 1994
5. Ain A. Son *The Physical Basis of Dimensional Analysis* MIT Cambridge, MA 02139, 2001
6. Goncharov, K. A. and Kolesnikov, V. Components Volume Ratio on LHP with Single and Several Evaporators, *The Aerospace Corporation, CPL'98 Workshop*, El Segundo, CA, USA, 2-3 March 1998
7. Luikov, A. V. *Heat and Mass Transfer in Capillary-Porous Bodies*, Pergamon Press, Oxford, 1966.
8. Chi, S.W. *Heat Pipe Theory and Practice*, McGraw-Hill, NY 1976
9. Dunbar, N. and Cadell, P. Working Fluids and Figures of Merit for CPL/LHP Applications, *The Aerospace Corporation, CPL-98 Workshop*, El Segundo, CA, USA, 2-3 March 1998.
10. Long, J. B., *Alternate working fluids for capillary driven two-phase loops*, MS Thesis, Clemson University, 2001.
11. Finlay, I. C., *The theory of heat pipes. Course papers: Analysis, Design and Manufacture of heat pipes*, Glasgow, 19-21 June 1973.
12. Ku, J. Operational Characteristics of Loop Heat Pipes *SAE Paper 1999-01-2007*, 1998.
13. Gerasimov, Yu. F., Maidanik, Yu. F., Dolgirev, Yu.E., Kiseev, V.M., Filippov, G.A., Starikov L.G., Some results of low-temperature antigravity heat pipes investigations *Journal of Engineering Physics and Thermophysics* , Vol. 30, No.4 pp. 581-586, 1976 (In Russian).
14. Wayner, P.C. Jr., Long Range Intermolecilar Forces in Change of Phase Heat Transfer, *Proc. 33rd National Heat Transfer Conf.*, Albuquerque, New Mexico USA, August 15-17 1999
15. Renk, F.J. and Wayner, P.C. Jr. An Evaporation Ethanol Meniscus. Part I: Experimental Studies *Heat transfer Transactions of the ASME* Vol. 101 pp. 55-62, 1985.
16. Mirzamogham, A.V. and Catton, I. Holographic Interferometry Investigation of enhanced Tube Meniscus Behavior *J. Heat transfer Transactions of the ASME* Vol. 110 pp. 208-213, 1988.
17. Rott, N., Note on the history of the Reynolds number, *Annual review of fluid mechanics* Vol. 22 pp. 1-11, 1990.
18. Demidov, A.S. and Yatsenko, E.S., Investigation of heat and mass transfer in the evaporation zone of heat pipe operating by the "inverted meniscus" principle, *Int. J. Heat Mass Transfer*, Vol. 37, No. 14, pp 2155-2163, 1994.

19. Kaya, T. and Hoang, T. T., Mathematical Modeling of LHPs and Experimental Validation," *J. Thermophysics and Heat Transfer*, Vol. 13, No. 3, pp. 314-320 1999.

20. Figus, C. Le Bray Y., Bories, S. and Prat M., Heat and Mass Transfer with Phase Change in a Porous Structure Partially Heated: Continuum Model and Pore Network Simulations *Int. J. Heat Mass Transfer*, Vol. 42, pp 2557-2569, 1999.

21. Schonberg J.A., DasGupta, S., Wayner, P.C. Jr., An Augmented Young-Laplace Model of an Evaporating Meniscus in Microchannel with High Heat Flux *Exp. Therm. And Fluid Sci.* Vol.10, pp 163-170, 1995.

22. Wang, J. and Catton, I., Evaporation heat transfer in biporous media, *Heat & Mass Transfer*, pp. 275-281, 2001.

23. Wayner, P.C. Jr., Kao, Y.K., LaCrox L.V. The interline heat-transfer coefficient of an evaporating wetting film *Int. J. Heat Mass Transfer* Vol. 19, pp. 487-492, 1976.

24. Sartre, V., Zaghdoudi, M.C., Lallemand M. Effect of Interfacial Phenomena on Evaporative Heat Transfer in Micro Heat Pipes *Int. J. Therm. Sci.* Vol. 39, pp.498-504, 2000.

25. Liao Q. and Zhao T.S. On capillary-driven flow and phase-change heat transfer in porous structure heated by finned surface: measurement and modeling *Int. J. Heat Mass Transfer* Vol. 43, pp 1141-1155, 2000.

26. Khrustalev D. and Faghri A., Heat Transfer in The Inverted Meniscus Type Evaporator at High Heat Fluxes *Int. J. Heat Mass Transfer,* Vol. 38, No. 16, pp.3091-3101, 1995.

27. Wei Qu and Tongze Ma, Effects of The Polarity of Working Fluids on Vapor -Liquid Flow and Heat Transfer Characteristics in a Capillary, *Microscale Thermophysical Eng.*, Vol. 6, pp. 191-207, 2002

28. Deraygin, B.V. and Zorin A.M., Optical Study of the Absotption and Surface condensation of Vapors in the Vicinity of Saturation on a Smooth Surface, *Proc. 2nd Int. Congr. Surface Activity*, London, 2, pp. 145-152., 1957.

29. Gad-el-Hak, M., *Flow Physics in The MEMS handbook* /edited by Mohamed Gad-el-Hak, CRC Press, Boca Raton London New York Washington, D.C. 2002.

30. Stralen, S. V. and Cole, R. *Boiling Phenomena: Physicochemical and Engineering Fundamentals and Applications*, Hemisphere, V.1, p.119-121 1979.

31. Dunn, P.D. and Reay, D.A., *Heat Pipes*, 3rd ed., Pergamon, NY 1982.

32. Marcus, B.D. Theory and Design Variable Conductance Heat Pipes, *NASA CR-2078* Washington DC. 1972.

33. Barthelemy, R.R., Evaporation heat transfer in heat pipes. *Proc. 2nd Int. Heat Pipe Conf.*, Bologna, p.425-437, 1976.

34. Peng, X.F., Peterson G.P. and Wang, B.X. Heat transfer characteristics of water flowing through microchannels *Experimental Heat Transfer* 7(4), p. 249-264, 1994.

35. Kwak, H.Y. and Panton, R.L. Tensile strength of simple liquids predicted by a model of molecular interactions, *J. Phys. D: Appl. Phys.*, V. 18 p.647-659. 1985.

36. Kwak, H.Y. and Lee, S. Homogeneous Bubble Nucleation Predicted by a Molecular Interaction Model, *Journal of Heat Transfer Transactions of the ASME*, V. 113 p.714-721. 1991.

37. Reid, R.C. Prausnitz, J.J. and Sherwood, T.K. *The properties of Gases and Liquids*, 3rd ed., McGraw-Hill, NY 1976.

38. Ku, Jentung Operational Characteristics of Loop Heat Pipes *SAE Paper 1999-01-2007*, 1998, 16 p.

39. Maidanik, Yu.F and Fershtater, Yu.G., Theoretical Basis and Classification of Loop Heat Pipes and Capillary Pumped Loops, *Proc. 11 Heat Pipe Conf.* 1997, X-7 15 p. 1997.

40. Goncharov K.A., Nikitkin M.N., Golovin O.A., Fershtater Yu.G. , Maidanik Yu.F., Piukov S.A., Loop Heat Pipes in Thermal Control Systems for "OBZOR" Spacecraft, 25th *Int. Conf. on Environmental Systems*, San Diego, California, July 10-13, Paper No. 951555, 1995.

41. Surguchev O.V., Elchin A.P., Goncharov K.A. A loop heat pipes application in thermoregulation systems of space apparatus for communication and the Earth remote sensors *Proc. 5th Minsk Int. Seminar "Heat Pipes, Heat Pumps, Refrigerators"*, Sept. 8-11, 2000 Minsk, Belarus 2003.

42. Baturkin V., Micro-Satellites Thermal Control – Concepts and Components, *Proc 4th IAA Symp. on Small Satellites for Earth Observation* April 7-11 Berlin Germany 2003.

43. Grigoriev, Y. I.; Grigorov, E. I.; Cykhotsky, V. M.; Prokhorov, Y. M., Two-Phase Heat Transport Loop of Central Thermal Control System of the Int. Space Station "Alpha" Russian Segment *AIChE Symp. Series* n.310, 9 p.1996.

44. Bednov S.M. Scientific and Engineering Aspects of Integration of Two-Phase Thermal Control Systems in spacecraft *31st Int. Conf. on Environmental Systems*, Orlando, Florida, USA, July 9-12, 2001.

45. Delil A.A.M. Two-Phase Experiment for the in orbit Demonstration of Two-Phase Heat Transport Technology *Adv. Space Res.* Vol. 16, No. 7 pp. (7)113-(7)112, 1995.

46. Chuang P.-Y. A., Cimbala J.M., Breziner J.S. Jr., Conroy C.T., El-Ganayni A.A., Riley D. R., Comparison of Experiments and 1-D Steady –State Model of a Loop Heat Pipe, *Proc. Int. Mech. Eng. Congress and Exp.* Nov 17-22, 2002 New Orleans, LA USA IMECE2002-33542 8p. 2002.

47. Perotto V., Tavera S., Goncharov K., Orlov A., Golovin O., 1500 W Deployable Radiator with Loop Heat Pipe *Proc. 4th Minsk Int. Seminar "Heat Pipes, Heat Pumps, Refrigerators"*, Sept. 4-7, 2000 Minsk, Belarus pp.23-29, 2000.

48. Keshock E.G. and Sadeghipour M.S. Analytical comparison of condensing flows inside tubes under earth gravity and space environments *Acta Astronautica* Vol.10, No.7, pp. 505-511, 1983.

49. Mishkinis D., Ochterbeck J. M., Sodtke C., Ku J., Butler D. Non-Dimensional Analysis and Scaling Issues in Loop Heat Pipes *41s Aerospace Science Meeting and Exhibit*, 6-9 Jan. Reno, Nevada, Paper AIAA-2003-0341, 12 p., 2003.

50. Dobson M.K. and Chato J.C., Condensation in Smooth Horizontal Tubes, *J. Heat Transfer* Vol. 120 pp. 193-213. 1998.

51. Mandhane J.M., Gregory J.A., and Aziz K., A Flow Pattern Map For Gas-Liquid Flow in Horizontal Pipes, *Int. J. Multiphase Flow*, Vol.1, pp. 537-555. 1974.

52. Taitel Y. and Dukler A.E., A Model for Prediction Flow Regime Transitions in Horisontal and Near Horisontal Gas-Liquid Flow, *AIChE J.* Vol. 22, No.1 pp.47-55, 1976.

53. Soliman H.M. On the Annular to Wavy Flow Pattern Transition During Condensation Inside Horisontal Tubes, *The Canadian J. Chem. Eng.*, Vol. 60 pp. 475-481, 1982.

54. Soliman H.M. Correlation of Mist-Annular Transition During Condensation, *The Canadian J. Chem. Eng.*, Vol. 61 pp. 178-182, 1983.

55. Hewitt G.H., Multiphase Fluid Flow and Pressure Drop. Gas-Liquid Flow in *Heat Exchanger Design Handbook* Hemisphere 1983.

56. Breber G., Palen J.W. and Taborek J. Prediction of Horizontal Tubeside Condensation of Pure Components Using Flow Regime Criteria *J. Heat transfer*, Vol. 102, Aug., pp. 471-476, 1980.

57. Chen I. Y., Brayant M., Sifuentes R., Brady T., Two-Phase Ammonia Pressure Drop in Horizontal Straight Tubes, *National Heat Transfer Conf.* Aug. 8-11, 1993, Atlanta, GA, pp. 150-162, 1993.

58. Galbiati L. and Andreini P., Transition between stratified and annular regimes for horizontal two-phase flow in small diameter tubes, *Int. Commun. Heat Mass Transfer* Vol. 19, No. 2 pp.185-190, 1992.

59. Yang C. Y. and Shien C.C., Flow Pattern of Air-Water and Two-Phase R-134a in Small Circular Tubes, *Int. J. Multiphase Flow* Vol. 27 pp. 1163-1177 2001.

60. Baker O., Design of Pipe Lines for Simultaneous Flow of Oil and Gas, *Oil and Gas J.* Vol. 26, July 1954.

61. Soliman H.M. and Azer N.Z., Visual Studies of Flow Patterns During Condensation Inside Horizontal Tubes, *Proc. 5th Int. Heat Transfer Conf.* Sept.3-7 1974 Tokyo, Japan, Vol. 3 pp. 241-245, 1983.

62. Zhao J.F., Xie J.C., Lin H., Hu W.R., Ivanov A.I., Belyaev A.Yu., Experimental Studies on Two-Phase Patterns Abroad the Mir Space Station, *Int. J. Multiphase Flow*, Vol.27, pp. 1931-1944, 2001.

63. Reinarts T.R., Ungar E. K. and Butler C.D. Adiabatic Two-Phase Pressure Drop in Microgravity: TEMP2A-3 Experiments and Comparison with Predictions, *Proc. of 33rd Aerospace Meeting and Exhibit*, Jan. 9-12, 1995 Reno, NV, AIAA paper 95-0635, 11 p. 1995.

64. Kachnik L., Lee D., Best F., Faget N., Microgravity Boiling and Convective Condensation Experiment *ASME Paper No. 87-WA/HT-12*, 1987.

65. Zhao L. and Rezkallah K.S., Gas-Liquid Flow Patterns at Microgravity Conditions, *Int. J. Multiphase Flow*, Vol.19, No. 5 pp. 751-763, 1993.

66. Colin C. and Fabre J., Gas-Liquid Pipe Flow Under Microgravity Conditions: Influence of Tube Diameter on Flow Patterns and Pressure Drops, *Adv. Space Res.* Vol. 16, No. 7 pp. (7)137-(7)142, 1995.

67. Keshock E. G., Lin C. S., Harrison M. E., Edwards L. G., Knapp J., and Zhang X., Measurement of Two-Phase Flow Characteristics Under Microgravity Conditions, *Proc. 4th Microgravity Fluid Physics and Transport Phenomena Conf.*, Aug. 12-14, 1998 Cleveland, Ohio USA, pp.14-20 1998.

68. Bousman W. S., *Studies of Two-Phase Gas-Liquid Flow in Microgravity*, Ph. D. dissertation, University of Houston. 1994.

69. Bousman W.S., McQuillen J.B., and Witte L.C., Gas-Liquid Flow Patterns in Microgravity: Effects of Tube Diameter, Liquid Viscosity and Surface Tension, *Int. J. Multiphase Flow*, Vol.22, pp. 1035-1053, 1996.

70. Balakotaiah V., Jayawardena S. S., and Nguyen L. T., Studies on Normal and Microgravity Annular Two-Phase Flows, *Proc. 4th Microgravity Fluid Physics and Transport Phenomena Conf.* Aug. 12-14, Cleveland, Ohio USA, pp.6-12 1998.

71. Reinarts T.R., *Adiabatic Two-Phase Flow Regime Data and Modeling for Zero and Reduced (Horizontal Flow) Acceleration Fields*, Ph. D. Thesis, Texas A&M University, College Station, TX, USA, 1993.

72. Chen I.Y., Downing R.S., Parish R., Keshock E., A Reduced Gravity Flight Experiment: Observed Flow Regimes and Pressure Drops of Vapor and Liquid Flow in Adiabatic Piping, *Proc. ASME 25th National Heat Transfer Conf.*, July 24-27, 1988, Houston, TX, pp.203-215, 1988.

73. T.R. Reinarts, E.K. Ungar, Prediction of Annular Two-Phase Flow in Microgravity and Earth-Normal Gravity Conditions, *Proc. of National Heat Transfer Conf.*, Houston, TX, Published in ASME HTD, Vol.92, No.310 pp.60-67, 1996.

74. Rezkallah K.S., Weber Number Based Flow-Pattern Maps For Liquid-Gas Flows at Microgravity, *Int. J. Multiphase Flow*, Vol.22, No.6 pp. 1265-1270, 1996.

75. Coddington P. and Macian R. A Study of the Performance of Void Fraction Correlations Used in the Context of Drift-Flux Two-Phase Flow Models *Int. meeting : Trends in Numerical and Physical Modeling for Industrial Multiphase Flows* Institut d'Etudes Scientifiques de Cargèse (Corse), France 27-29 11 p. Sept. 2000.

76. Lowe D.C. and Rezkallah K.S., Flow Regime Identification in Microgravity Two-Phase Flows Using Void Fraction Signals *Int. J. Multiphase Flow*, Vol.25, pp. 433-457, 1999.

77. Crowley C.J., Scaling of Multiphase Flow Regimes and Interfacial Behavior at Microgravity, *Proc. 4th Microgravity Fluid Physics and Transport Phenomena Conf.*, Aug. 12-14, 1998 Cleveland, Ohio USA, pp.919-929 1998.

78 Jayawardena S.S., Balakotaiah V., Witte L.C., Flow Pattern Transition Maps For Microgravity Two-Phase Flow. *AIChE J.* Vol. 43 pp. 1637-1640, 1997.

79. Lee D., *Thermodynamic and Flow Regime Analysis for Condensing Two-Phase Flow in Microgravity Environment,* Ph. D Thesis, Texas A&M University, College Station , TX 1987.

80. Zhao J.F. and Hu W.R., Slug to Annular Flow Transition on Microgravity Two Phase Flow *Int. J. Multiphase Flow*, Vol. 26, pp. 1295-1304, 2000.

81. Tronievski L. and Ulbrich R., Two-Phase Flow in Rectangular Channels *Chem. Eng. Sci.* Vol. 39 No. 4 pp. 751-765, 1984.

82. Taitel Y. and Dukler A.E., A Theoretical Approach to the Lochart- Martinelli Correlation for Stratified Flow, *Int. J. Multiphase Flow*, Vol. 2, pp. 591-595, 1976.

83. Bergelin O.P. and Gazley C., Co-current Gas-Liquid Flow in Horizontal Tubes *Proc. Heat Transf. And Fluid Mech. Inst.* Vol. 29 pp. 5-8 1949.

84. Crowley C.G., Izenson M.G., Barry J.J., Martin J.L., Ent R.S. and Valenzuela J.L., *Design Manual for Microgravity Two-Phase Flow and Heat Transfer* Final Report from Creare Inc. to Air Force Astronautics Laboratory, Report No. AL-TR-89-027, 1989.

85. Beattie D.R.H. and Whalley P.B., A Simple Two-Phase Frictional Pressure Drop Calculation Method *Int. J. Multiphase Flow,* Vol. 8, No.1 pp. 83-87, 1982.

86. Chen I., Downing R., Keshock E.G., Al-Sharif M., Measurements and Correlation of Two-Phase Pressure Drop Under Microgravity Conditions *J. Thermophysics* Vol. 5 No.4 pp. 514-523, 1991.

87. Tronievski L. and Ulbrich R., Two-Phase Gas-Liquid Flow: Authors Reply *Chem. Eng. Sci.* Vol. 40 No. 10 pp. 2000-2002, 1985.

88. Kawahara A., Chung P.M.-Y., Kawaji M., Investigation of Two-Phase Flow Pattern, Void Fraction and Pressure Drop in a Microchannel *Int. J. Multiphase Flow*, Vol. 28, pp. 1411-1435, 2002.

89. Sciascia V.M. and Duncan A.B., Characterization of Earth-Gravity Two-Phase Flow in Strait Tubing and 180° Tubing Bends for Microgravity Environment System Design. *National Heat Transfer Conf.*, Houston, TX, Published in ASME HTD, Vol.92, No.310 pp. 73-82, 1996.

90. Srindar K.R., Chao B.T. and Soo S.L., Pressure Drop in Fully Developed, Turbulent, Liquid-Vapor Annular Flows on Zero Gravity, *AIAA J.* Vol.30, No.4, pp. 1016-1026 1992.

91. Zhao L. and Rezkallah K.S., Pressure Drop in Gas-Liquid Flow at Microgravity Conditions *Int. J. Multiphase Flow*, Vol.21, No. 5 pp. 837-849, 1995.

92. Collier J.G. *Convective Boiling and Condensation*, McGraw-Hill, 421 p. 1972.

93. Wallis G.B. *One-Dimensional Two-Phase Flow*, McGraw-Hill, 409 p. 1969.

94. Ohadi M.M., Li S.S., Rademacher R. and Dessiatoun S., Critical Review of Available Correlation for Two-Phase Flow Heat Transfer of Ammonia Int. *J. Refrig.* Vol. 19 No. 4 pp. 272-284, 1996.

95. Chepurenko V.P. Lagutin A.E. Gogol N.I., An Investigation of Heat Exchange During Condensation a Pipe at Low Heat Flow Densities , Energy Efficiency in Refrigeration and Global Warming Impact, *Proc. Refrig. Sci. and Techn.*, Belgium, May 1993, Int. Inst. Of Refrig., Comissions B1/2 pp.243-249, 1993.

96. Cavallini A. and Zecchin R., A Dimensionless Correlation for Heat Transfer in Forced-Convective Condensation, *Proc. of 5th Int. Heat Transfer Conf.*, Japan Society of Mechanical Engineers, Vol. 3 pp. 309-313, 1974.

97. Vrable D.L., Yang W.-J. and Clark J.A., Condensation of Refrigerant-12 Inside Horizontal Tubes with Internal Axial Fins, *Proc. of 5th Int. Heat Transfer Conf.*, Japan Soc. of Mech. Eng., Vol. 3 pp. 250-254, 1974.

98. Shah M.M., A General Correlation for Heat Transfer During Film Condensation Inside Pipes, *Int. J. Heat and Mass Transfer* Vol. 22 pp.547-556.1979.

99. Fujii T., Enhancement to Condensing Heat Transfer – New Developments, *J. Enhanced Heat Transfer* Vol. 2 Nos.1-2 pp.127-137 1995.

100. Chen S.L., Gerner F.M. and Tien C.L., General Film Condensation Correlations, *Experimental Heat Transfer*, Vol.1 pp.93-107, 1987.

101. Shah M.M., Heat Transfer During Film Condensation in Tubes and Annuli: a Review of Literature *ASHRAE Trans.* Vol.87, No.1, pp.1086-1105, 1981.

102. Ackers W.W. and Rosson H.F., Condensation Inside Horizontal Tube *Chem. Eng. Prog. Symp. Series* Vol. 56 No.30 pp.145-149 1960.

103. Azer N.Z., Two-Phase Flow in *1993 ASHRAE Handbook – Fundamentals*, ASHRAE Atlanta GA 1993.

104. Tandon T.N. Varma H.K. and Gupta C.P., Heat Transfer During forced Convection Condensation Inside Horisontal Tube, *Int. J. Refrigeration*, Vol.18 No. 3 pp.210-214, 1995.

105. Dobson M.K., *Heat Transfer and Flow Regimes During Condensation in Horizontal Tubes,* Ph.D. Thesis Depart. of Mech. and Ind. Eng. University Illinois at Urbana Champaign 1994.

106. Rosson H.F. and Meyers J.A. Point Values of Condensing Film Coefficients Inside Horizontal Tubes *Chem. Eng. Prog. Symp. Series* Vol. 61 No.59 pp. 190-199.1965.

107. Chato J.C., Laminar Condensation Inside Horizontal and Inclined Tubes *ASHRAE J.* Vol.4 pp. 52-60. 1962.

108. Jaster H. and Kosky P.G., Condensation Heat Transfer in a Mixed Flow Regime, *Int. J. Heat and Mass Transfer* Vol. 19 pp.95-99 1976.

109. Best F.R., Kachnik L. and Lee D.J., Space Microgravity Two Phase Flow Safety Considerations *Trans. of the American Nuclear Society*, Vol.52 pp.489-490.